



Sphingolipid changes do not underlie fatty acid-evoked GLUT4 insulin resistance nor inflammation signals in muscle cells^S

Nicolas J. Pillon,^{1,*} Scott Frendo-Cumbo,^{1,†} Maya R. Jacobson,[†] Zhi Liu,[†] Paul L. Milligan,[§] Hai Hoang Bui,[§] Juleen R. Zierath,^{*,**} Philip J. Bilan,[†] Joseph T. Brozinick,[§] and Amira Klip^{2,†}

Departments of Physiology and Pharmacology* and Molecular Medicine and Surgery** Integrative Physiology, Karolinska Institutet, Stockholm, Sweden; Program in Cell Biology,[†] Hospital for Sick Children, Toronto, Ontario, Canada; and Eli Lilly and Company,[§] Indianapolis, IN

ORCID ID: 0000-0003-1107-9490 (N.J.P.)

Abstract Ceramides contribute to obesity-linked insulin resistance and inflammation *in vivo*, but whether this is a cell-autonomous phenomenon is debated, particularly in muscle, which dictates whole-body glucose uptake. We comprehensively analyzed lipid species produced in response to fatty acids and examined the consequence to insulin resistance and pro-inflammatory pathways. L6 myotubes were incubated with BSA-adsorbed palmitate or palmitoleate in the presence of myriocin, fenretinide, or fumonisin B1. Lipid species were determined by lipidomic analysis. Insulin sensitivity was scored by Akt phosphorylation and glucose transporter 4 (GLUT4) translocation, while pro-inflammatory indices were estimated by IκBα degradation and cytokine expression. Palmitate, but not palmitoleate, had mild effects on Akt phosphorylation but significantly inhibited insulin-stimulated GLUT4 translocation and increased expression of pro-inflammatory cytokines *Il6* and *Ccl2*. Ceramides, hexosylceramides, and sphingosine-1-phosphate significantly heightened by palmitate correlated negatively with insulin sensitivity and positively with pro-inflammatory indices. Inhibition of sphingolipid pathways led to marked changes in cellular lipids, but did not prevent palmitate-induced impairment of insulin-stimulated GLUT4 translocation, suggesting that palmitate-induced accumulation of deleterious lipids and insulin resistance are correlated but independent events in myotubes. **We propose that muscle cell-endogenous ceramide production does not evoke insulin resistance and that deleterious effects of ceramides *in vivo* may arise through ancillary cell communication.**—Pillon, N. J., S. Frendo-Cumbo, M. R. Jacobson, Z. Liu, P. L. Milligan, H. Hoang Bui, J. R. Zierath, P. J. Bilan, J. T. Brozinick, and A. Klip. **Sphingolipid changes do not underlie fatty acid-evoked GLUT4**

insulin resistance nor inflammation signals in muscle cells. *J. Lipid Res.* 2018. 59: 1148–1163.

Supplementary key words ceramides • lipidomics • inflammation • glucose transporter 4

Obesity is associated with accumulation of deleterious lipid intermediates, including ceramides and diacylglycerol (DAG), in adipose tissue, liver, and skeletal muscle (1). This lipotoxic fat accumulation contributes to low-grade local inflammation and the development of insulin resistance and cardiovascular complications of obesity. Elevations in several sphingolipid species in plasma and tissues have been associated with type 2 diabetes mellitus, dyslipidemia, and atherosclerosis. The plasma sphingolipid species associated with lipoproteins and albumin are emerging as biomarkers for metabolic diseases (2, 3).

Ceramides are elevated in patients with type 2 diabetes and a body of work considers them to be direct contributors to insulin resistance (4). Independently of a possible important role for sphingolipids in plasma, liver, or other tissues, it is unclear and still confounding whether intracellular ceramide accumulation in muscle cells is causally related to insulin

Abbreviations: CE, cholesteryl ester; C2C12-GLUT4myc, mouse C2C12 muscle cells with stable expression of *myc*-tagged glucose transporter 4; DAG, diacylglycerol; FB1, fumonisin B1; FDR, false discovery rate; GLUT4, glucose transporter 4; GLUT4myc, *myc*-tagged glucose transporter 4; GM3, ganglioside GM3; LPC, lysophosphatidylcholine; L6-GLUT4myc, rat L6 muscle cells with stable expression of *myc*-tagged glucose transporter 4; PA, palmitate solution coupled to BSA; PC, phosphatidylcholine; PE, phosphatidylethanolamine; PI, phosphatidylinositol; PO, palmitoleate solution coupled to BSA; PS, phosphatidylserine; qPCR, quantitative PCR; Sa1P, sphinganine-1-phosphate; S1P, sphingosine-1-phosphate; TAG, triacylglycerol.

¹N. J. Pillon and S. Frendo-Cumbo contributed equally to this work.

²To whom correspondence should be addressed.

e-mail: amira@sickkids.ca

S The online version of this article (available at <http://www.jlr.org>) contains a supplement.

This work was supported by a Foundation Grant from the Canadian Institutes of Health Research (A.K.), H2020 Marie Skłodowska-Curie Actions Fellowship Grant 704978 (H2020-MSCA-IF-2015) (N.J.P.), and a Natural Sciences and Engineering Research Council of Canada Alexander Graham Bell Canada Graduate Scholarship-Doctoral (S.F.C.). The authors declare no financial conflicts of interest.

Manuscript received 25 September 2017 and in revised form 26 April 2018.

Published, *JLR Papers in Press*, May 23, 2018

DOI <https://doi.org/10.1194/jlr.M080788>

Copyright © 2018 by the American Society for Biochemistry and Molecular Biology, Inc.

This article is available online at <http://www.jlr.org>

resistance. Indeed, ceramide content is elevated in liver and adipose tissue from high-fat-fed animals, but it is controversial whether ceramides accumulate in skeletal muscle during obesity and diabetes, and whether they lead to muscle-specific and whole-body insulin resistance (5). Some studies find elevated net levels of total ceramides in the skeletal muscle of diet-induced insulin-resistant mice and humans (6–8), but many report no change in muscle ceramide content in human and mouse models of obesity and type 2 diabetes (9–11), often despite significant increases in plasma and liver ceramide content (12, 13). This dissociation of changes in skeletal muscle ceramide levels from changes in insulin sensitivity questions the role for muscle ceramides in mediating fat-induced insulin resistance (5).

Glucose transporter 4 (GLUT4) translocation is the fundamental process sustaining insulin-dependent glucose uptake, and this step fails in obesity and type 2 diabetes. In spite of its importance, the effect of ceramides on GLUT4 translocation in muscle has not been examined. In vitro studies using mouse C2C12 or rat L6 muscle cells consistently show that exposure to the saturated fatty acid, palmitate, but not the unsaturated oleate, increases overall ceramide content (14–17). Early studies using inhibitors of serine palmitoyltransferase or ceramide synthase suggested that inhibition of sphingolipid formation could reverse palmitate-induced insulin resistance in muscle cells (18–20), while others reported no change in insulin sensitivity after silencing of serine palmitoyltransferase, the rate limiting step of ceramide synthesis (21), or overexpressing ceramide synthases (22). All of those studies were performed in either mouse C2C12 or rat L6 cells using largely different concentrations of palmitate (0.2–1.2 mM) and incubation times (6–48 h), and most used only Akt Ser⁴⁷³ phosphorylation as a readout for insulin signaling, which makes comparisons and interpretation difficult. Importantly, GLUT4 translocation to the membrane was not examined vis a vis ceramide content or synthesis.

Here, we used a well-established insulin-sensitive muscle cell culture system and performed lipidomic analysis to exhaustively explore whether saturated fatty acids selectively alter the muscle cell sphingolipid profile, and if so, whether these species contribute to pro-inflammatory outcomes and to insulin resistance of GLUT4 translocation in a cell-autonomous manner. We hypothesized that modulating the abundance of different intermediates of the sphingolipid pathway would influence fatty acid-induced insulin resistance, focusing on GLUT4 translocation and pro-inflammation indices.

METHODS

Reagents

Myriocin, fumonisin B1 (FB1), and fenretinide were from Milipore (Etobicoke, ON, Canada). DL-threo-PDMP (PDMP) and sphingosine kinase inhibitor 2 (SKI-II) were from Cayman Chemicals (Ann Arbor, MI). Antibodies used were specific for: total Akt (1:1,000; Cell Signaling #2920), pSer⁴⁷³-Akt (1:1,000; Cell Signaling #4060), pThr³⁰⁸-Akt (1:1,000; Cell Signaling #9275), pSer176/180-IKK α / β (1:1,000; Cell Signaling #2697), total IKK β (1:1,000; Cell Signaling #2684), total IKK α (1:1,000; Cell Signaling #2682), pSer-IkB α (1:1,000; Cell Signaling #9246), total IkB α (1:1,000;

Cell Signaling #9242), pSer-p65 (1:1,000; Cell Signaling #3033), total p65 (1:1,000; Cell Signaling #3034), β -actin [1:10,000; Sigma-Aldrich (St. Louis, MO) A5441], and actinin-1 (1:10,000; Sigma-Aldrich A5044). Other chemicals were from Sigma-Aldrich.

Palmitate and palmitoleate solution preparation

Solutions of fatty acids were complexed to BSA as described previously (23). Briefly, fatty acids were dissolved in 50% ethanol and then diluted 25 times in a 10.5% BSA solution. These stock solutions were further diluted in cell culture media (16-fold dilution), exposing the cells to a final concentration of 0.5 mM palmitate/palmitoleate and/or 0.12 mM BSA (final lipid:BSA ratio of 4:1). Palmitate and palmitoleate solutions thus coupled to BSA are denoted as PA and PO, respectively, hereafter.

Cell culture

Rat L6 muscle cells with stable expression of *myc*-tagged GLUT4 (L6-GLUT4 myc) were grown in α -MEM supplemented with 10% FBS, 100 units/ml penicillin, 100 μ g/ml streptomycin, and 250 ng/ml amphotericin B. Differentiation into myotubes was induced by switching confluent cells to α -MEM supplemented with 2% FBS for 4–7 days. Mouse C2C12 muscle cells with stable expression of *myc*-tagged GLUT4 (C2C12-GLUT4 myc) were grown and differentiated as described previously (24).

Lipid extraction

Lipids were extracted using one phase extraction with methanol-dichloromethane. Internal standard mixture was added to the samples before extraction. Lipid levels were quantified by the ratio of analyte and internal standard and calibration curves were obtained by serial dilution of a mixture of lipid standards. Pure synthetic standards of sphingolipids were purchased from Avanti Lipids. Isotope-labeling synthetic standards were synthesized internally at Eli Lilly and Company. For lipidomic analysis, 572 ng D₅-triacylglycerol (TAG) 16:0/16:0/16:0; 2 mg phosphatidylcholine (PC) 14:0/14:0; 287 ng sphingomyelin 17:0; 40 ng ¹³C₁₈-oleic acid; 108 ng PC 15:0/15:0; and 60 ng DAG 15:0/15:0 of standards were added to 200 μ l of mixture after extraction.

Lipidomics

Lipidomics was conducted via flow injection ESI/MS/MS using an AB-Sciex 5600 TripleTOF system (AB Sciex, Framingham, MA). The mass spectra are acquired in two stages. In the first stage the TOF spectra was scanned with minimal collision energy from 100 to 1,200 Da with high resolution. The second stage consisted of TOF product ion scans of 611 precursor masses from 349.199 to 959.809 isolated with a resolution of 0.7 Da and changed stepwise in 1.001 Da increments. Sphingomyelins were identified and distinguished from PC isotopes by unfragmented proton adducts during the first stage. The remaining lipids were identified in the second stage by precursor and product ion pairs predicted by the analyte species and lipid class.

Sphingolipid measurement

Specific analysis of ceramides and sphingolipids was performed by LC/ESI/MS/MS using an AB Sciex 6500 quadrupole mass spectrometer equipped with an ESI probe and interfaced with the Agilent 1290 infinity LC system (Agilent, Palo Alto, CA). The UPLC system consisted of an Agilent 1290 binary pump, thermostat, TCC, and sampler. The injection volume was 10 μ l per extracted sample. Sphingolipids were separated with a Poroshell 120 EC-C8 column, 2.1 \times 50 mm, 2.7 μ m (Agilent). Mobile phase A was water:methanol:formic acid:ammonium formate (45/55/0.5%/5 mM, v/v). Mobile phase B was acetonitrile:methanol:formic acid:ammonium formate (50/50/0.5%/5 mM, v/v). The valve,

sample loop, and needle were washed with acetonitrile:methanol (50/50, v/v) for 20 s. Mass spectrometric analyses were performed online using ESI/MS/MS in the positive mode.

Nomenclature

The nomenclature for the lipidomics analysis was designed to reflect what is known about the samples without making any claims about what is not known. For TAGs, we detected the precursor mass, which was used to determine the sum of the three acyl groups, and the product mass, which was used to determine the fragment after one complete acyl chain is removed. As a result, the nomenclature reads: [known acyl chain]_[precursor mass]_TAG_C[sum of all carbons in three acyl chains]:[sum of all double bonds in three acyl chains]. For example, "18:1 TAG 878 C52:1" has a precursor mass of 878.7, which means it has three acyl chains with a total of 52 carbons and 1 double bond (52:1). The fragment ion (579.5) means the fragment has 34 carbons and no double bonds, which in turn guarantees that one of the acyl chains is an 18:1 chain (the difference between them). Overall this molecule is likely a TAG 18:1, 18:0, 16:0, but there are contributions from less probable analytes, such as TAG 18:1, 20:0, 14:0.

Cell surface GLUT4myc

L6-GLUT4myc myotubes grown in 96-well plates were serum deprived for 2 h and then treated with or without insulin (100 nM, 30 min). The cell surface density of GLUT4myc was measured as described previously (25).

RNA isolation and quantitative PCR

All reagents were from Life Technologies (Carlsbad, CA). RNA was isolated using TRIzol® and cDNA synthesized using the SuperScript VILO® cDNA kit. Quantitative PCR (qPCR) was done using predesigned TaqMan probes. HPRT1 and ABT1 expression was not affected by any of the treatments, and they were therefore used as housekeeping genes. qPCR was performed for 40 cycles (95°C for 1 s, 60°C for 20 s) and the relative quantity of mRNA was calculated using the $\Delta\Delta Cq$ method.

Immunoblotting

After treatments, cells were scraped into lysis buffer (20 mM Tris-HCl, 138 mM NaCl, 2.7 mM KCl, 1 mM MgCl₂, 2.5% glycerol, and 1% Nonidet-P40) supplemented with protease and phosphatase inhibitors (5 mM EDTA, 1 mM Na₃VO₄, 20 mM NaF, 1 mM dithiothreitol, and protein inhibitor cocktail; Sigma-Aldrich) and protein content was measured by the BCA assay. For Western blotting, proteins were boiled in Laemmli buffer, separated by SDS-PAGE, and transferred onto PVDF membrane (Bio-Rad, Hercules, CA). Membranes were then blotted using primary antibodies (4°C overnight) and washed, and peroxidase-coupled secondary antibody (1:10,000) was applied for 1 h at room temperature. Membranes were revealed using ECL (Bio-Rad), visualized using an Odyssey Fc Imager (LI-COR, Lincoln, NE), and quantified using Odyssey Fc Image Studio version 4.0 (LI-COR).

Statistical analysis

Lipidomics data were analyzed using R software (www.r-project.org). The sphingolipid and lipidomic analyses were normalized according to the common species measured in both methods and merged (676 analytes in total). Mislabeled species, species with more than 10% missing values, and compounds with values 100-fold lower than the median of the whole dataset were excluded. The remaining missing values were imputed using nearest neighbor averaging. The final data containing 384 lipid species was log₂ transformed, scaled, and analyzed using *t*-test and Bonferroni corrected false discovery rate (FDR). Other analyses were performed using

Prism software (GraphPad Software, San Diego, CA). Results from inhibitor experiments were compared by two- or three-way ANOVA followed by Fisher's LSD post hoc tests. Statistical significance was set at $P < 0.05$.

RESULTS

Palmitate, but not palmitoleate, impairs insulin-induced GLUT4 translocation and activates pro-inflammation indices in muscle cells

Insulin stimulates glucose uptake into muscle through activation of a signaling cascade typified by dual phosphorylation of the serine/threonine kinase Akt that culminates in translocation of the glucose transporter, GLUT4, to the cell membrane (26). This process is recapitulated in myotubes of the rat L6 cell line stably transfected with GLUT4myc for easy detection of the translocation process (27). Within 20 min, insulin elevated surface GLUT4 levels by 1.6-fold, and this response was dwarfed by an 18 h preexposure of the myotubes to the saturated fatty acid, PA (0.5 mM) (Fig. 1A). Notably, parallel preexposure to the mono-unsaturated fatty acid, PO (0.5 mM) did not cause insulin resistance. L6 myotubes therefore react to saturated fatty acid exposure by developing insulin resistance.

We recently reported that L6 myotubes also respond selectively to PA, but not to PO, by mounting a cell-autonomous activation of the pro-inflammatory pathway governed by the transcription factor, NFκB (23). Indeed, L6 myotubes exposed to PA, but not PO, elevated the expression of the chemokine, *Ccl2/MCP1*, and the cytokine, *Il6* (Fig. 1B, C).

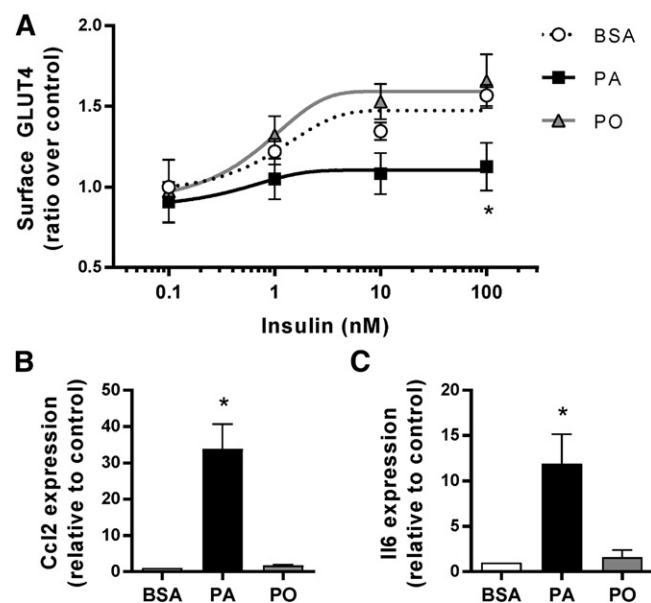


Fig. 1. Palmitate, but not palmitoleate, impairs insulin action and activates inflammatory signals. L6 myotubes were exposed to 0.5 mM PA, PO, or the BSA vehicle for 18 h and then stimulated with 100 nM insulin for 20 min. A: Surface GLUT4 was measured as described in the Methods (n = 4; * $P < 0.05$ vs. BSA control). B, C: *Ccl2* and *Il6* expression was measured by qPCR (n = 3; * $P < 0.05$ vs. BSA control).

Hence, L6 myotubes reproduce two cardinal responses that arise *in vivo* during high-fat feeding with saturated fatty diets: activation of pro-inflammatory programs and development of insulin resistance (28).

Palmitate and palmitoleate differentially elevate lipid content in L6 myotubes

Lipidomic analysis of L6 myotubes exposed to either PA or PO was performed to monitor changes in lipid species. A primary component analysis (Fig. 2A) showed that PA, PO, and the BSA vehicle cluster apart from each other, suggesting that they induce selective changes in lipid content. This was confirmed on a heat map (Fig. 2B) where most of the results of PA experiments clustered together and away from those with PO or BSA incubations. A Venn diagram (Fig. 2C) demonstrated that 200 lipid species significantly changed in response to cellular incubation with either PA or PO (FDR < 0.01). Among them, 79 were selectively changed by PA, 74 specifically by PO, and 47 were modified under either PA or PO conditions. The compounds most significantly elevated in response to PA were various species of TAG, dihydroceramides, ceramides, and sphingosine-1-phosphate (S1P) (Fig. 2D). In comparison, PO seemed to partition mostly toward triglyceride species (Fig. 2E). All statistically significant changes in lipid species after cellular treatments with PA or PO are presented in supplemental Table S1.

Calculation of the total amount of each class of lipids (Fig. 2F) revealed that both PA and PO increased the total amount of lysophosphatidylcholine (LPC) and TAG, although the fatty acyl chain composition differed, with 16:1 and 16:0 species being enriched in response to PO and PA, respectively (supplemental Table S1). Only PO, but not PA, increased the amount of cholesteryl esters (CEs), while phosphatidylinositols (PIs) were specifically increased by PA. No changes were detected in the total amount of DAGs, PC, phosphatidylethanolamine (PE), and phosphatidylserine (PS). A detailed analysis of all sphingolipid species (Fig. 2G) demonstrated that both PA and PO treatments elevated sphinganine, sphinganine-1-phosphate (Sa1P), deoxysphinganine, dihydroceramides, and S1P. Only PA augmented ceramides and hexosylceramides. Gangliosides were significantly reduced by both PA and PO and only PO was able to elevate the levels of sulfatide. Sphingosine, lactosylceramides, and sphingomyelins were not affected by any of the fatty acid treatments.

A few enzymes of the sphingolipid pathway, such as ceramide synthase, are upregulated in adipose tissue from obese individuals (29). We therefore hypothesized that fatty acids would regulate the expression of one or several enzymes in the sphingolipid pathway that could lead to the changes observed in cellular lipid composition. However, neither PA treatment nor PO treatment of myotubes induced changes in the expression of the enzymes, serine palmitoyltransferase (*Spt2*), ceramide synthases (*Cers1*, *Cers4*, *Cers6*), dihydroceramide desaturases (*Degs1*, *Degs2*), sphingomyelin phosphodiesterases (*Smpd1*, *Smpd2*, *Smpd3*), acid ceramidases (*Asah1*, *Asah2*), or alkaline ceramidases (*Acer1*, *Acer2*, *Acer3*) (supplemental Fig. S1A, B). These data suggest

that the PA- and PO-induced changes in sphingolipid content were due to mechanisms independent of changes in gene expression of the main determining enzymes. We therefore proceeded to inhibit the enzymatic activity of the different enzymes of the sphingolipid pathway (supplemental Fig. S1C). Along with the treatments with PA or PO, L6 myotubes were systematically exposed to the serine palmitoyltransferase inhibitor, myriocin, the ceramide synthase inhibitor, FB1, and the dihydroceramide desaturase inhibitor, fenretinide. Under each condition, insulin sensitivity and the pro-inflammatory response were measured and cells were extracted for lipidomic analysis. As expected, myriocin, FB1, and fenretinide altered diverse sphingolipid species, but importantly, did not affect other DAGs, TAGs, or phosphatidyl species (supplemental Fig. S2).

Inhibition of the *de novo* pathway does not reverse palmitate-induced insulin resistance of GLUT4 translocation and inflammation

Myotubes were pretreated with myriocin (25 μ M) for 30 min and then incubated with PA or PO in the presence of myriocin for 18 h to inhibit serine palmitoyltransferase, the first and rate-limiting step of the *de novo* ceramide synthesis pathway. Inhibition of serine palmitoyltransferase blunted the PA-induced increase in sphinganine, Sa1P, deoxysphinganine, dihydroceramides, ceramides, hexosylceramides, and ganglioside GM3 (GM3). Myriocin did not significantly affect the amount of lactosylceramides, sphingosine, S1P, and sphingomyelins (Fig. 3A). Importantly, and despite a significant attenuation of the PA-induced changes in lipid composition, myriocin did not reverse the PA-induced insulin resistance of GLUT4 translocation in either L6-GLUT4myc (Fig. 3B) or C2C12-GLUT4myc myotubes (Fig. 3C). Myriocin also did not reverse the expression of the pro-inflammatory cytokines, *Il6* and *Ccl2* (Fig. 3D, E).

Fenretinide is a potent inhibitor of dihydroceramide desaturase, the final step of the ceramide synthesis pathway. Contrary to myriocin, incubation of L6 myotubes with fenretinide led to a significant accumulation of sphinganine and dihydroceramide (Fig. 4A). Similar to myriocin, fenretinide induced a 60% decrease in ceramides and blunted the PA-induced increase in hexosylceramides (Fig. 4A). Overall, fenretinide significantly reduced ceramides and hexosylceramides, but at the expense of a marked accumulation of dihydroceramide and sphinganine. Interestingly, fenretinide significantly increased the accumulation of deoxysphinganine. Importantly, with this switch in sphingolipid composition, fenretinide had no effect on GLUT4 translocation (Fig. 4B). The effect of fenretinide on the pro-inflammatory axis was complex. The expression of *Il6* was not affected by fenretinide alone and PA still exerted a lower, but significant, induction of this gene (Fig. 4C). On the other hand, the drug itself promoted *Ccl2* expression, and consequently PA had no further action in the presence of the inhibitor (Fig. 4D). Overall, effectively inhibiting dihydroceramide desaturase did not prevent PA-induced insulin resistance or an acknowledged index of pro-inflammatory responses.

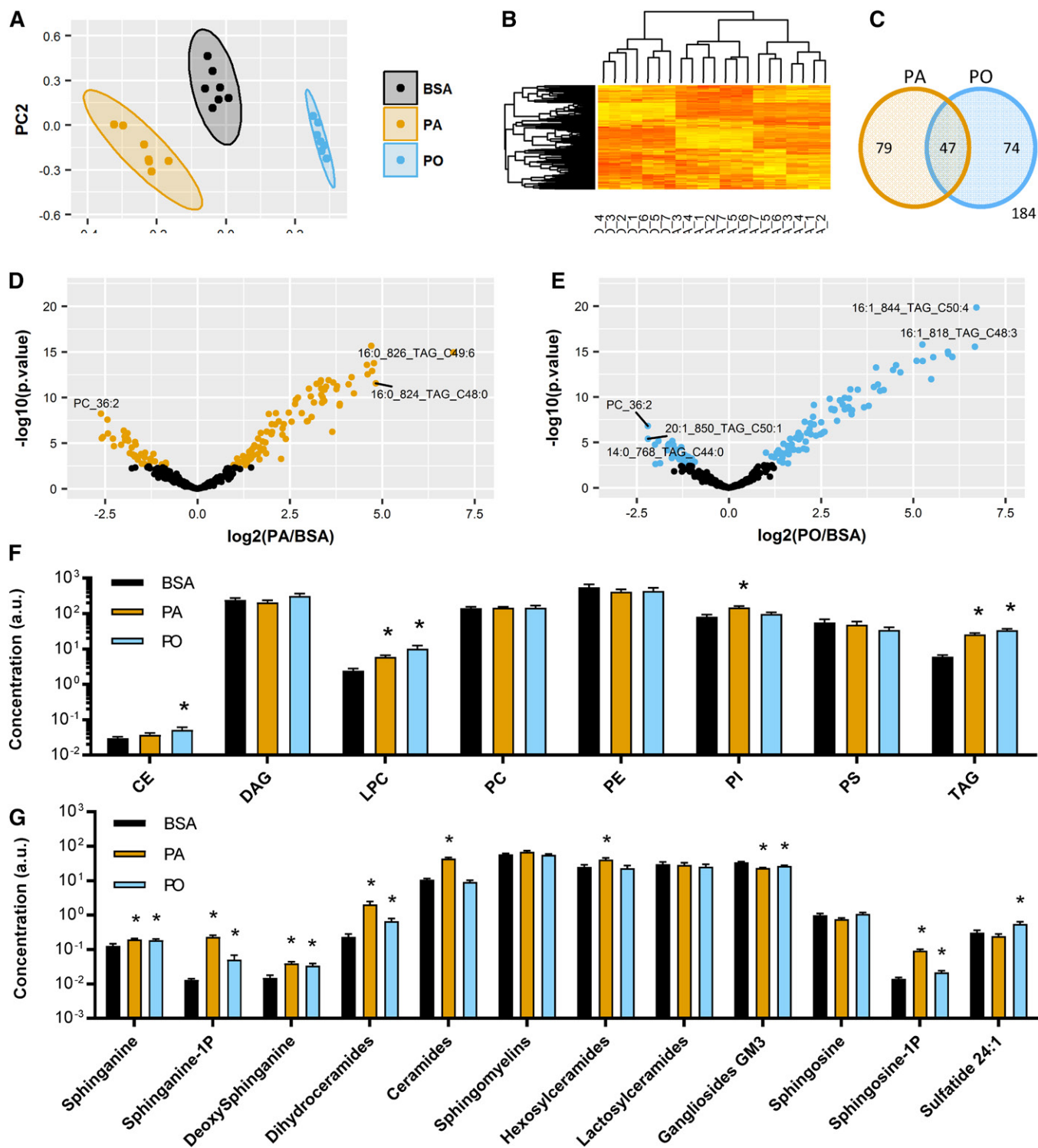


Fig. 2. Lipidomic analysis reveals selective increases in lipid species by palmitate and palmitoleate. L6 myotubes were exposed to 0.5 mM PA, PO, or the BSA vehicle for 18 h. Cells were extracted and lipidomic analysis performed as described in the Methods ($n = 7$). **A:** Primary component analysis comparing PA, PO, and BSA groups. **B:** Heat map showing clustering of all lipid species and treatment groups. **C:** Venn diagram showing overlap of significantly changed lipid species (t -test, $FDR < 0.01$) after treatment with PA or PO compared with the BSA control. Individual species are available in Tables 1 and 2. **D, E:** Volcano plots of lipid species induced by the treatment with PA or PO. The colored dots pass the threshold for statistical significance ($FDR < 0.01$, t -test). **F, G:** Sum of lipid species by families (t -test vs. BSA control, $*P < 0.05$).

Inhibition of ceramide synthase does not reverse palmitate-induced insulin resistance and inflammation

FB1 inhibits ceramide synthase, an enzyme contributing to ceramide accumulation from the de novo and salvage

pathways (29). Incubation of L6 myotubes with fatty acids in the presence of FB1 (50 μ M) led to significant elevations in sphinganine, deoxysphinganine, and S1P with drops in dihydroceramides, ceramides, and hexosylceramides

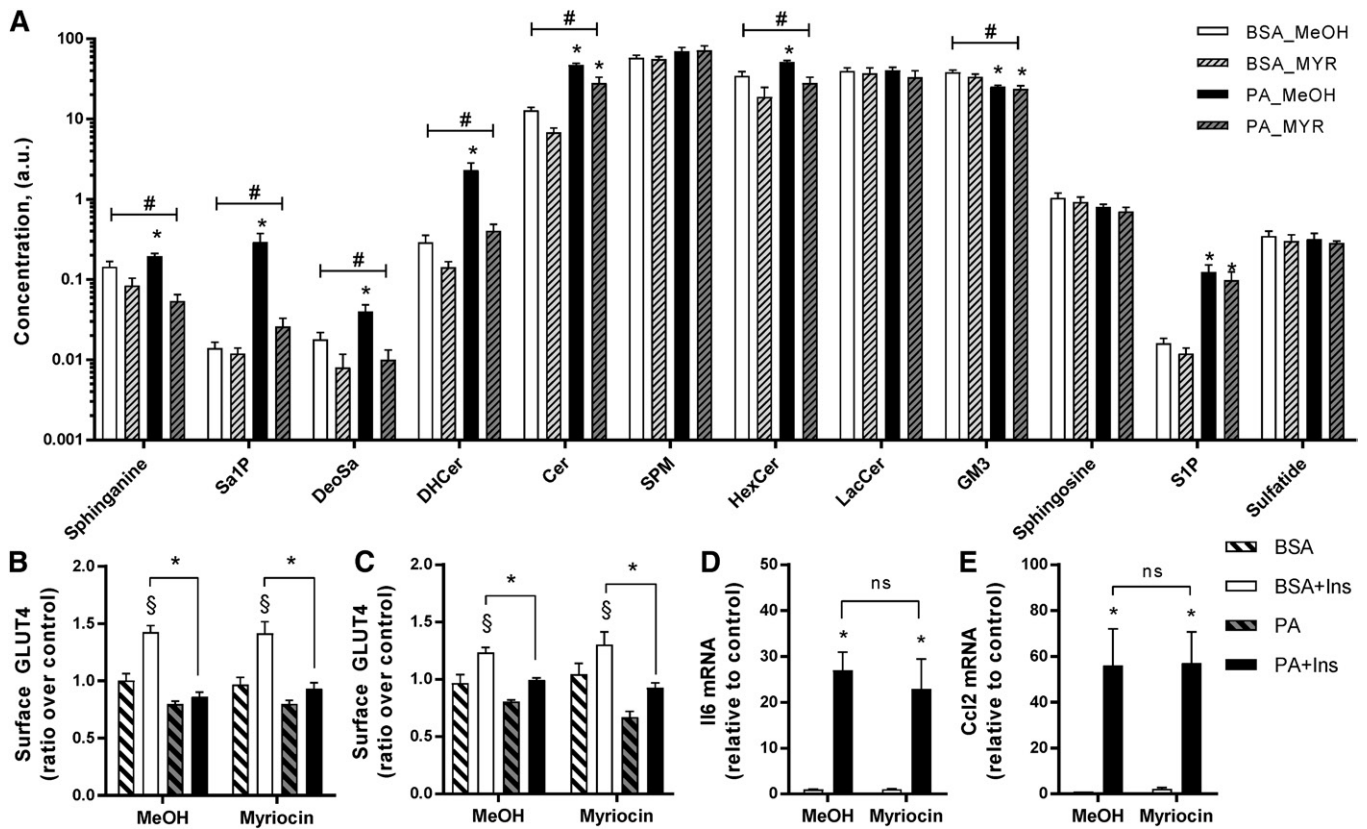


Fig. 3. Inhibition of the de novo pathway with myriocin does not reverse palmitate-induced insulin resistance and inflammation. Myotubes were pretreated with myriocin (25 μ M) or the methanol (MeOH) vehicle for 30 min and then incubated with 0.5 mM PA in the presence of myriocin for 18 h. **A:** Lipid species were measured in L6 myotubes using lipidomic analysis as described in the Methods ($n = 7$). **B:** Surface GLUT4 was measured in L6-GLUT4myc myotubes as described in the Methods [$n = 7$; three-way ANOVA (insulin, PA, myriocin)]. **C:** Surface GLUT4 was measured in C2C12-GLUT4myc myotubes as described in the Methods [$n = 3$; three-way ANOVA (insulin, PA, myriocin)]. **D, E:** Expression of *Ccl2* and *Il6* in L6 myotubes after PA and myriocin exposure was measured by qPCR [$n = 4$; two-way ANOVA (PA, myriocin)]. #Overall significant effect of inhibitor (two-way ANOVA; $P < 0.05$; $n \geq 5$). *Significant effect of PA over BSA control (two-way ANOVA; $P < 0.05$). §Significant effect of insulin over unstimulated control ($P < 0.05$). DHCer, dihydroceramide; HexCer, hexosylceramide; SPM, sphingomyelin; LacCer, lactosylceramide; MYR, myriocin.

(Fig. 5A). Despite these effects on specific sphingolipid species, FBI did not prevent the PA-induced reduction of insulin-stimulated GLUT4 translocation or cell-autonomous inflammation (Fig. 5B–D). Hence, inhibiting ceramide synthase does not prevent insulin resistance or the pro-inflammatory responses evoked by PA.

Palmitate, but not palmitoleate, inhibits insulin-induced Akt activation and activates NF κ B signaling

A partial inhibition of Akt phosphorylation is typically observed in the muscles of human and mouse models with insulin resistance, particularly on Thr³⁰⁸ (30, 31); although it is not necessarily the only cause for reduced glucose uptake and GLUT4 translocation (32–34). Though insulin-induced phosphorylation of Akt on Ser⁴⁷³ is commonly measured (35), phosphorylation on Thr³⁰⁸ correlates better with Akt activity and is most relevant for insulin-stimulated GLUT4 translocation (36). Even then, a substantial inhibition of Akt phosphorylation (>80%) is required to consequently observe reduced GLUT4 translocation in muscle cells (32) and adipocytes (37). Here, we show that phosphorylation of both sites was stimulated by insulin in

myotubes and dose-dependently reduced in the presence of PA (Fig. 6A, B). Only the highest concentration of PA (0.8 mM) decreased insulin-induced phosphorylation of Akt close to baseline levels, but this dose was toxic to the cells and therefore associated with confounding effects beyond the changes in lipid composition.

Activation of the muscle cell pro-inflammatory NF κ B pathway requires activation of the kinase, IKK, and phosphorylation and degradation of the I κ B α inhibitory subunit, followed by translocation of the p65 subunit to the nucleus where it regulates the expression of inflammatory cytokines. Confirming this behavior, PA, but not PO, dose dependently increased the phosphorylation of the IKK complex, phosphorylation and degradation of I κ B α , and phosphorylation of p65 (Fig. 6A, B). As in the case of GLUT4 translocation and cytokine expression shown above, myriocin did not reverse the deleterious effect of PA on insulin-induced phosphorylation of Akt on Ser⁴⁷³ and Thr³⁰⁸ and did not affect the PA-triggered degradation of I κ B α (Fig. 6C–F).

On the other hand, the dihydroceramide desaturase inhibitor, fenretinide, reversed the PA-induced impairment of insulin-induced Akt signaling on Thr³⁰⁸, but had no

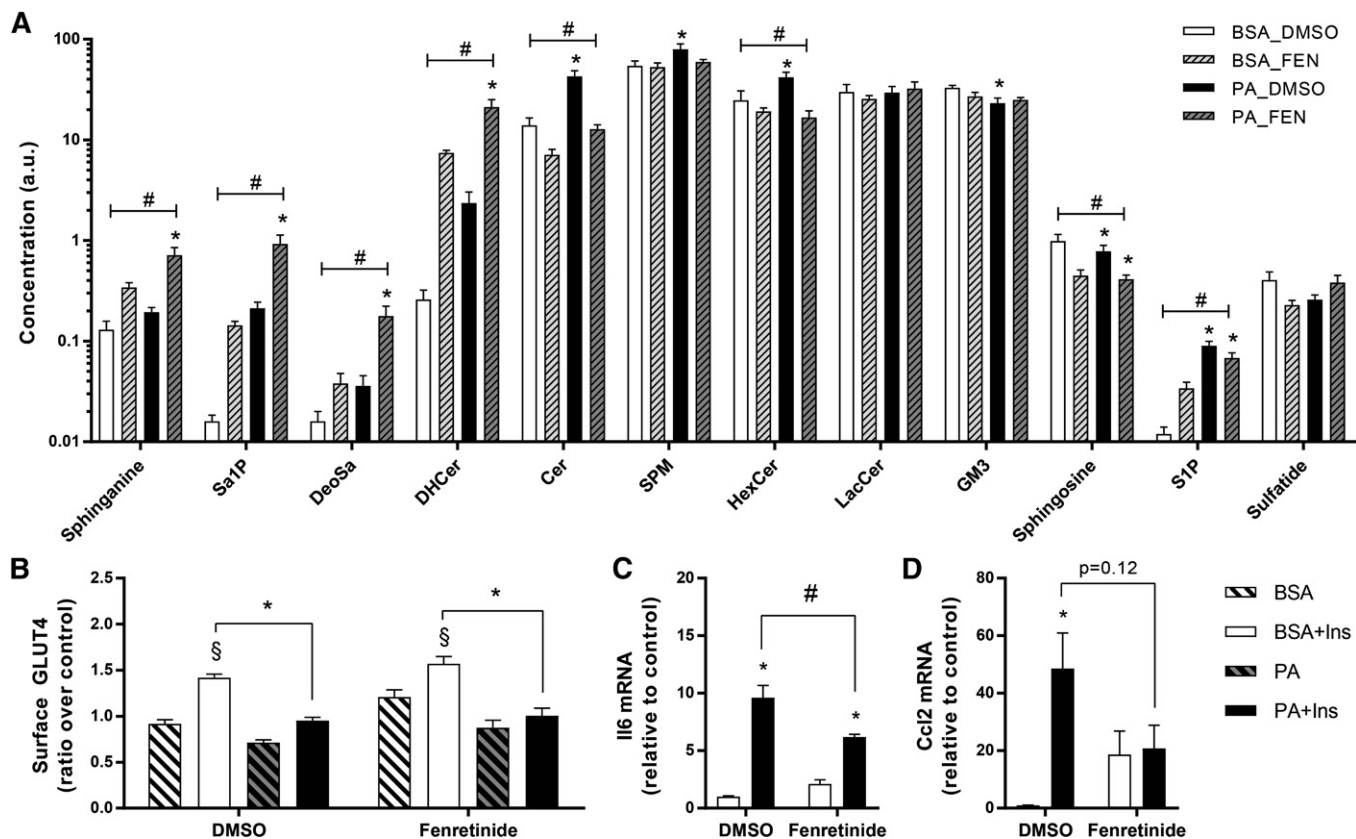


Fig. 4. Inhibition of the de novo pathway with fenretinide does not reverse palmitate-induced insulin resistance, but reduces palmitate-induced inflammation. L6 myotubes were pretreated with fenretinide (10 μ M) for 30 min and then incubated with 0.5 mM PA in the presence of fenretinide for 18 h. **A:** Lipid species were measured using lipidomics as described in the Methods. **B:** Surface GLUT4 was measured as described in the Methods [$n = 9$; three-way ANOVA (insulin, PA, fenretinide)]. **C, D:** Expression of *Ccl2* and *Il6* after PA and fenretinide exposure was measured by qPCR [$n = 7$; two-way ANOVA (PA, fenretinide)]. #Overall significant effect of inhibitor (two-way ANOVA; $P < 0.05$). *Significant effect of PA over BSA control (two-way ANOVA; $P < 0.05$). §Significant effect of insulin over unstimulated control ($P < 0.05$). DHCer, dihydroceramide; HexCer, hexosylceramide; SPM, sphingomyelin; LacCer, lactosylceramide; FEN, fenretinide.

effect on the phosphorylation of Ser⁴⁷³ (Fig. 6G–J). Fenretinide, on its own, promoted I κ B α degradation, and consequently PA had no further action in the presence of the inhibitor (Fig. 6G–J), which paralleled *Ccl2* expression. Nonetheless, although fenretinide affected the various outcomes differently, it did not reverse the PA-elicited insulin resistance of GLUT4 translocation (Fig. 4B) or Ser⁴⁷³-Akt or the rise in *Il6* expression. FB1 did not prevent the PA-induced reduction of insulin-stimulated Thr³⁰⁸-Akt phosphorylation and I κ B α degradation, although it partially reversed the impaired Ser⁴⁷³-Akt phosphorylation (Fig. 6K–N). Therefore, and interestingly, the effects of this drug further reveal that the PA-induced inhibition of GLUT4 translocation is unrelated to the lipid's evoked reduction of Ser⁴⁷³-Akt phosphorylation.

Correlation of individual lipid species with insulin sensitivity and inflammation

Despite no significant reversion of the deleterious effects of PA in most parameters measured, the modulation of sphingolipid content had subtle effects on basal and insulin-induced responses as well as pro-inflammatory responses. Multi-parameter analysis of the different variables implicated in fatty acid responses therefore allowed

for the identification of lipid species associated with biological responses. The lipid species that showed the best correlation with pro-inflammatory index, defined here as $\frac{Il6 + CCL2}{I\kappa B\alpha}$, or compounded insulin sensitivity, defined here as $[\Delta\text{-change}(GLUT4 \times Akt_{Ser473} \times Akt_{Thr308})]$, are shown in **Fig. 7A, B**. Elevated TAG, ceramides, PI, and S1P were associated with a higher pro-inflammation index; among these, the most significant ones correlated with lower insulin sensitivity. This suggests that storage of lipids in these forms is deleterious for the cells and confirms the concept that increased ceramide or TAG content is associated with insulin resistance in vivo. Conversely, GM3, DAG, and PE were associated with a lower pro-inflammation index and higher insulin sensitivity, suggesting that accumulation of lipid in this form might provide some benefit to the cells. CEs were not significantly associated with insulin sensitivity, but correlated positively with inflammation. Finally, hexosylceramides and dihydroceramides were not significantly associated with inflammation, but negatively correlated with insulin sensitivity.

To further mine the information from the lipidomic analysis, the change in every individual lipid species induced by PA was plotted against its correlation to each

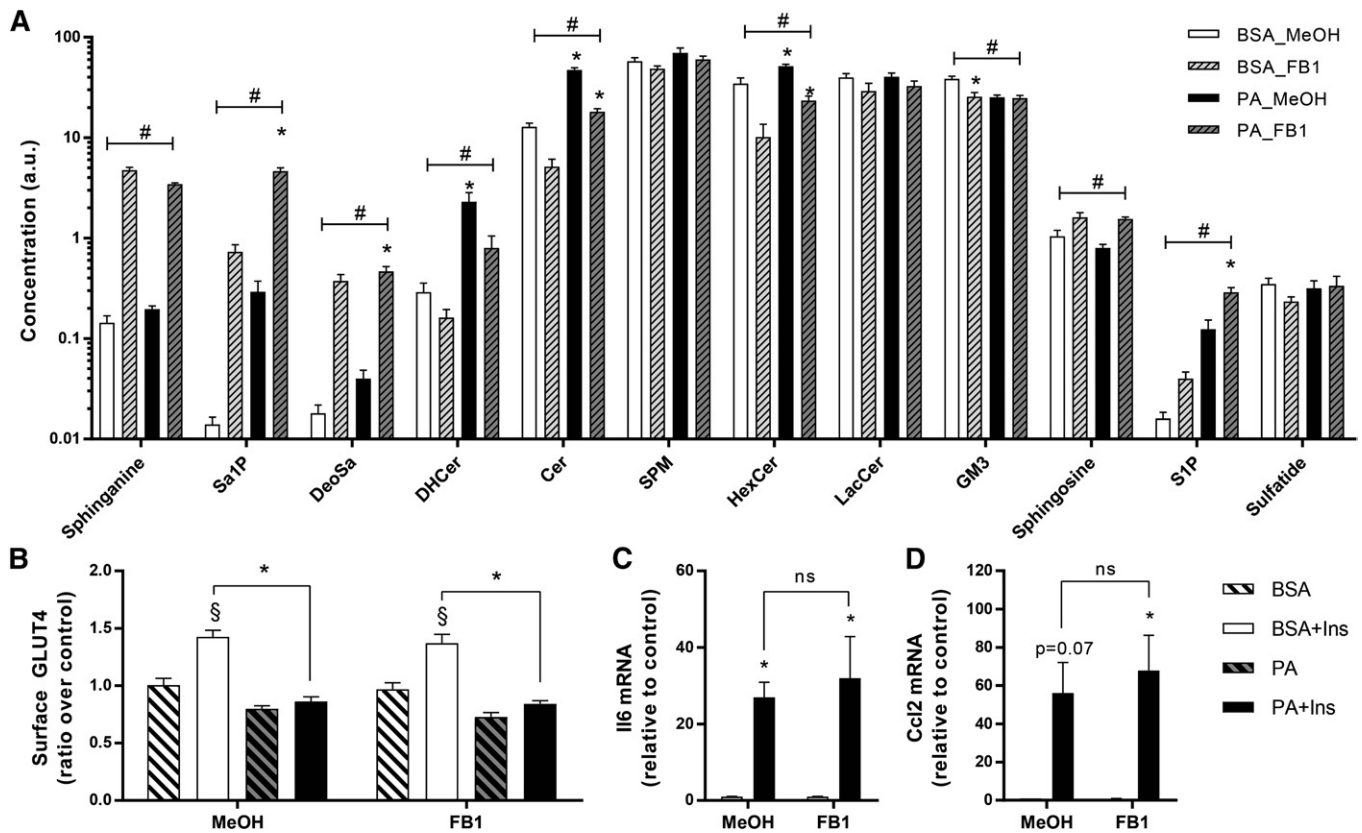


Fig. 5. FB1 does not reverse palmitate-induced insulin resistance and inflammation. L6 myotubes were pretreated with FB1 (50 μ M) for 30 min and then incubated with 0.5 mM PA in the presence of FB1 for 18 h. **A:** Lipid species were identified by lipidomics as described in the Methods. **B:** Surface GLUT4 was measured as described in the Methods [$n = 7$; three-way ANOVA (insulin, PA, FB1)]. **C, D:** Expression of *Ccl2* and *Il6* after PA and FB1 exposure was measured by qPCR [$n = 4$; two-way ANOVA (PA, FB1)]. #Overall significant effect of inhibitor (two-way ANOVA; $P < 0.05$). *Significant effect of PA over BSA control (two-way ANOVA; $P < 0.05$). §Significant effect of insulin over unstimulated control ($P < 0.05$). DHCer, dihydroceramide; HexCer, hexosylceramide; SPM, sphingomyelin; LacCer, lactosylceramide; MeOH, methanol.

parameter. A Venn diagram revealed an important overlap between lipid species that correlated with $I\kappa B\alpha$ degradation, cytokines, Akt phosphorylation, and GLUT4 translocation with many species associated with all four parameters (Fig. 7C). Only six species were independently associated with Akt activation, six species independently associated with GLUT4 translocation, and three species associated with both (Table 1), while not associated with pro-inflammation parameters. Fifteen species were associated specifically with NF κ B activation ($1/I\kappa B\alpha$), 32 associated with cytokine expression, and 4 associated with both NF κ B activation and cytokine expression independently of insulin sensitivity (Table 2). The presence of different species of TAG in all groups suggests that the composition of the different fatty acid branches may be more biologically relevant than the total amount of TAG.

Because PO had no effect on insulin sensitivity and pro-inflammation index, we focused on the 79 species that were specifically altered by PA (Fig. 2C, supplemental Table S1), represented as colored dots in Fig. 7D–G. The majority of lipid species elevated by PA correlated negatively with insulin-induced GLUT4 translocation (delta-change; Fig. 7D) and Akt activation (delta-change, average of Ser⁴⁷³ and Thr³⁰⁸, Fig. 7E), or correlated positively with cytokine expression (average of *Ccl2* and *Il6*; Fig. 7F) and NF κ B

activation ($1/I\kappa B\alpha$; Fig. 7G). There was a striking absence of compounds that would be associated with insulin resistance or inflammation and reduced by PA. On the other hand, there was no clear pattern as to which species induced by the unsaturated PO were positively or negatively associated with insulin sensitivity and inflammation (data not shown). Altogether, the correlation analysis revealed that most lipid species elevated by PA are associated with both insulin resistance and pro-inflammation. It also shows that higher ceramide and TAG levels are associated with insulin resistance. Importantly, this analysis does not link the deleterious effects of PA to a single lipid species or family of species.

The same analysis performed after classification of saturated versus unsaturated species did not reveal any differences in the level of unsaturation, pro-inflammatory action, or insulin sensitivity (data not shown). However, PA exposure led to a rise in most 16:0 species and 16:1-containing LPC and TAG, with a concomitant drop in 16:1-DAG (Fig. 8A). Given that TAGs are considered to be metabolically inert lipids, while DAG may have deleterious effects, our results reveal that a saturated acyl chain in DAG correlates better with insulin resistance than the equivalent monounsaturated DAG. Exposing cells to PO augmented 16:1-containing TAG, LPC, DAG, CE, and ceramides, but also diminished several 16:0 species, such as dihydroceramide,

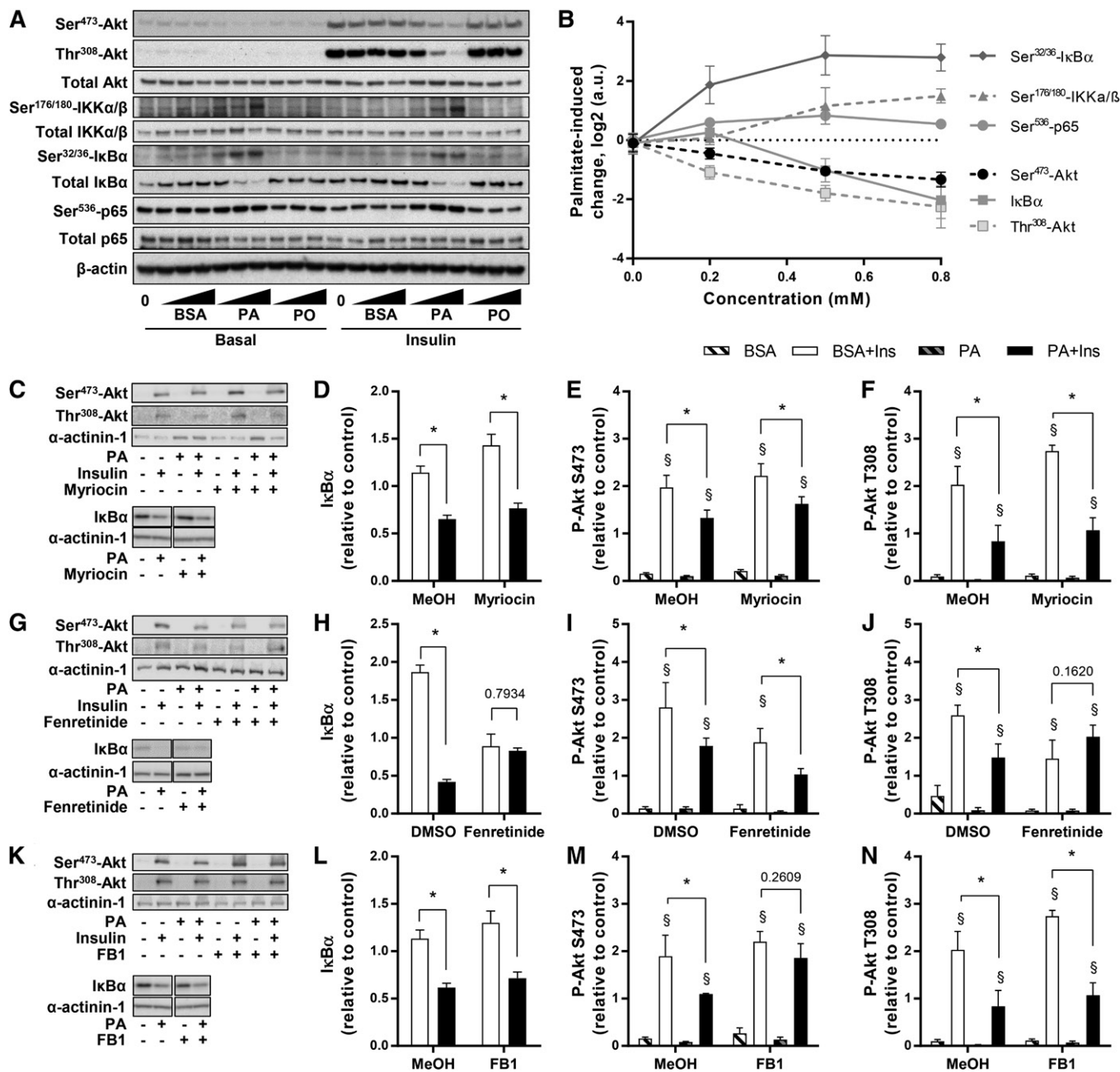


Fig. 6. Insulin and inflammatory signaling pathways. **A, B:** L6 myotubes were exposed to 0, 0.2, 0.5, or 0.8 mM PA or PO for 18 h, serum starved for 2 h, and stimulated with 2 nM insulin for 10 min. Akt, IKK, IκBα, and p65 were measured using specific antibodies. **C–F:** Effect of PA and myriocin was measured by Western blot for insulin-stimulated phosphorylation of Akt [$n \geq 3$; three-way ANOVA (insulin, PA, myriocin)] and degradation of IκBα [$n = 6$; two-way ANOVA (PA, myriocin)]. **G–J:** Effect of PA and fenretinide was measured by Western blot for insulin-stimulated phosphorylation of Akt [$n \geq 3$; three-way ANOVA (insulin, PA, fenretinide)] and degradation of IκBα [$n = 6$; two-way ANOVA (PA, fenretinide)]. **K–N:** Effect of PA and FB1 was measured by Western blot for insulin-stimulated phosphorylation of Akt [$n \geq 3$; three-way ANOVA (insulin, PA, FB1)] and degradation of IκBα [$n = 6$; two-way ANOVA (PA, FB1)]. *Significant effect of PA over BSA control (two-way ANOVA; $P < 0.05$). §Significant effect of insulin over unstimulated control ($P < 0.05$). MeOH, methanol.

LPC, and TAG, suggesting that some of the PO taken up might be desaturated into 16:0 in the cells. Interestingly, 16:1-containing DAGs were the only species regulated by PA and PO in an opposite manner and the only species positively associated with insulin sensitivity (Fig. 8B) and negatively associated with pro-inflammation index (Fig. 8C). The 16:1-containing TAG and LPC had opposite association with pro-inflammation index and insulin sensitivity, suggesting that only the incorporation of PO in DAG might

be beneficial. Altogether, these findings suggest that accumulation of 16:1 in DAG species might be favorable to dampen inflammation and promote insulin sensitivity.

DISCUSSION

Whether intracellular ceramide accumulation in myotubes plays a causal role in insulin resistance is a question

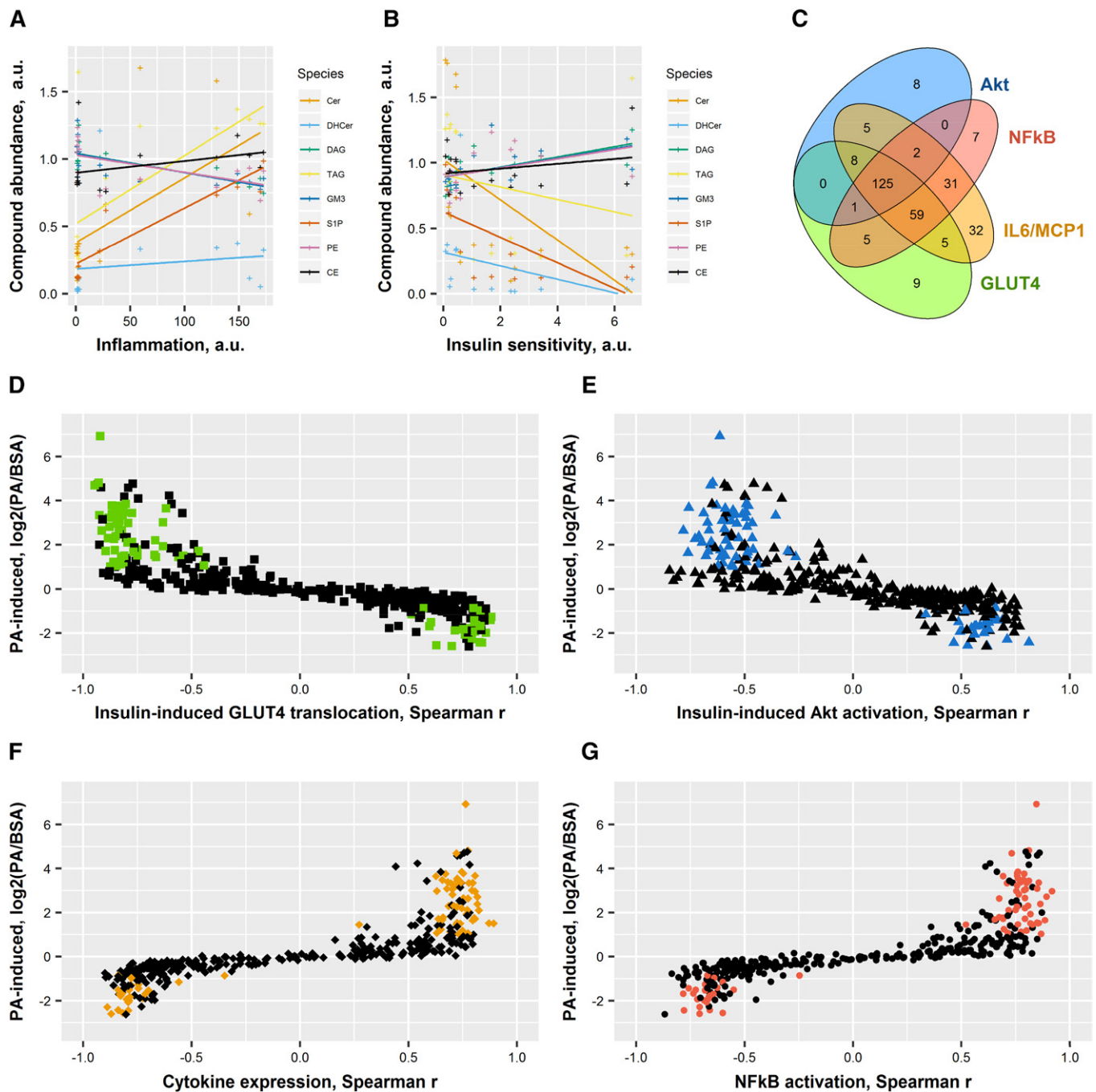


Fig. 7. Correlations between lipid species, insulin sensitivity, and inflammation. Spearman correlations were drawn between each individual compound and the measurements of insulin sensitivity (surface GLUT4 and Akt activation) and inflammation (*Il6*, *Ccl2* expression, and $I\kappa B\alpha$). Colored dots are the 79 species significantly increased specifically by PA. A: Species changed by PA and correlated with inflammation [$(Il6 + Ccl2)/I\kappa B\alpha$]. B: Species changed by PA and correlated with insulin sensitivity ($GLUT4 \times Ser^{473} \times Thr^{308}$). C: Venn diagram showing overlap between the different parameters for every individual species. D: Species changed by PA and correlated with GLUT4 translocation. E: Species changed by PA and correlated with Akt activation (average Ser^{473} and Thr^{308}). F: Species changed by PA and correlated with cytokine expression (average *Ccl2* and *Il6*). G: Species changed by PA and correlated with NFκB activation ($1/I\kappa B\alpha$). Individual values are presented in Tables 1 and 2. Cer, ceramide; DHCer, dihydroceramide.

that is difficult to assess in vivo where multiple organs communicate to regulate lipid homeostasis, insulin sensitivity, and pro-inflammatory responses. Using the simple insulin-responsive model of L6-GLUT4myc myotubes, we modulated the lipid composition using specific fatty acids and specific inhibitors of the sphingolipid pathway, and demonstrate that PA-induced accumulation of deleterious lipid species and insulin resistance are correlated, but independent,

events in skeletal muscle cells. Only PA, but not PO, induced the accumulation of ceramides, impaired insulin-induced Akt phosphorylation and GLUT4 translocation, and activated the NFκB signaling pathway and pro-inflammatory cytokine expression.

We used a nutrient-dependent approach to increase intracellular ceramides by exposing L6 myotubes to BSA-complexed fatty acids. Under these conditions, the uptake

TABLE 1. Lipid species specifically correlated with insulin sensitivity

	PA		PO		Akt		GLUT4	
	logFC	FDR	logFC	FDR	Spearman <i>r</i>	Spearman <i>P</i>	Spearman <i>r</i>	Spearman <i>P</i>
14:0_818_TAG_C48:3	0.36	2.85E-01	2.30	1.03E-08	-0.68	1.88E-02	-0.62	3.73E-02
16:1_818_TAG_C48:3	0.86	8.40E-02	6.67	2.67E-14	-0.19	5.58E-01	-0.67	2.04E-02
16:1_844_TAG_C50:4	0.82	1.56E-02	6.71	4.04E-18	-0.28	3.79E-01	-0.60	4.28E-02
18:0_TAG_C52_880-341	-0.05	9.20E-01	-0.12	8.05E-01	-0.29	3.54E-01	-0.64	3.01E-02
20:1_934_TAG_C56:1	-0.40	3.05E-01	-0.46	2.37E-01	0.62	3.48E-02	0.17	6.04E-01
HexCer_18:0	-0.72	1.84E-01	-0.36	5.67E-01	0.17	5.88E-01	0.61	4.00E-02
HexCer_24:0	-0.71	1.76E-01	-0.43	4.48E-01	0.32	3.08E-01	0.71	1.21E-02
LacCer_16:0	0.00	9.93E-01	-0.66	2.22E-01	-0.62	3.73E-02	-0.15	6.35E-01
PI_32:2	-0.47	3.17E-01	5.25	3.29E-13	0.73	9.05E-03	0.11	7.33E-01
PI_32:3	0.37	4.30E-01	-0.18	7.45E-01	-0.85	7.72E-04	-0.24	4.57E-01
PI_36:1	0.23	6.47E-01	-1.14	9.44E-03	-0.61	4.00E-02	-0.25	4.30E-01
PI_38:1	0.23	6.02E-01	-0.45	2.78E-01	-0.61	4.00E-02	-0.62	3.73E-02
PS_40:2	-0.87	1.51E-01	-0.93	1.25E-01	0.62	3.48E-02	0.65	2.59E-02
SaIP	4.09	8.17E-11	1.59	4.56E-04	-0.25	4.30E-01	-0.83	1.72E-03
Sphingosine	-0.38	2.63E-01	0.13	7.37E-01	0.65	2.59E-02	0.31	3.19E-01

HexCer, hexosylceramide; LacCer, lactosylceramide. Bold font indicates significance ($P < 0.05$).

of either PA or PO is equivalent and around 10 $\mu\text{mol/h}$, and 0.5 mM of PA does not affect cell viability in myotubes (23). Differences in lipid composition after PA or PO treatment would therefore not be due to cell death or a differential rate of uptake. Ceramides are composed of a sphingosine core plus a fatty acid chain. One of the two fatty acid chains is usually palmitate (16:0) and the second one of various lengths with or without unsaturations. This vast diversity of ceramide species complicates the study of their biological effects, as it is plausible that individual species selectively affect metabolic responses. Our lipidomics approach detected a total of 494 compounds, including 11 ceramide species, hexosylceramides, lactosylceramides, and sphingomyelins, providing an extensive map of the lipid composition after PA and PO exposure. Both PA and PO increased sphingolipid species in the de novo pathway down to dihydroceramides, but only PA elevated ceramides and hexosylceramides. In addition to sphingolipids, PA and PO also induced selective and significant changes in several TAG species. Among 200 species significantly affected by either PA or PO, only 29 species were similarly changed by PA and PO (significantly and in the same direction), demonstrating that different fatty acids can selectively modify cellular lipid content. Accumulation of ceramides within the myotubes can be due to: 1) increased flux of fatty acids into the sphingolipid pathway; 2) an increased amount of the biosynthetic or salvage pathway enzymes or decreased levels of the degradative enzymes; or 3) altered activity of these enzymes. We did not observe any difference in the mRNA levels of enzymes involved in the sphingolipid pathway, and the accumulation of deoxysphinganine after PA and PO treatments suggested an increased metabolic flux through serine palmitoyltransferase. Our data therefore suggest that PA and PO regulate the sphingolipid content by either modifying the flux of substrates into the pathway and/or the activity of the enzymes. Interestingly, human diabetics as well as animals fed a high-fat diet show significant increases in C18:1 deoxysphinganine, which have been suggested as biomarkers for the metabolic syndrome (38, 39). Exposure of myotubes to PA and PO

therefore resembles that feature observed in vivo in metabolic diseases.

Ceramides are not always associated with insulin resistance in vitro

In our hands, pharmacological modulation of serine palmitoyltransferase with myriocin, ceramide synthase with FB1, or dihydroceramide desaturase with fenretinide in L6 myotubes led to significant changes in PA-induced cellular sphingolipid composition; but despite these marked changes, none of the inhibitors prevented PA-induced impairment of GLUT4 translocation. These inhibitors prevented the formation of hexosylceramides by palmitate; and further, the hexosylceramide synthase inhibitor, PDMP, did not prevent PA-induced impairment of GLUT4 translocation either (supplemental Fig. S1A). As a caveat, however, PDMP can raise ceramide levels, not by substrate accumulation, but rather by inhibition of 1-*O*-acylceramide synthase, so the role of hexosylceramide synthase in the context of fatty acid exposure will require further investigation. PA exposure reduced Akt phosphorylation on both Ser⁴⁷³ and Thr³⁰⁸, but restoration of aspects of this inhibition by fenretinide (Thr³⁰⁸) or FB1 (Ser⁴⁷³) did not suffice to restore GLUT4 translocation. These results indicate that PA-induced insulin resistance of GLUT4 translocation is not associated to effects on one, or maybe either, phosphorylation site on Akt.

Surprisingly, a number of lipid species still showed positive or negative correlations with Akt phosphorylation, GLUT4 translocation, or inflammatory responses, demonstrating that a plethora of changes in lipid species are associated, though not necessarily causally, with the metabolic responses of the cells. This is the case for SIP, which has been previously associated with inflammatory responses, although in our hands, inhibition of sphingosine kinase did not reverse palmitate-induced insulin resistance and inflammation (supplemental Fig. S1B). Most compounds significantly heightened by PA correlated negatively with insulin sensitivity and positively with pro-inflammatory indices, suggesting that PA triggered a globally deleterious

TABLE 2. Lipid species specifically correlated with inflammation

	PA		PO		NFκB		Cytokines	
	logFC	FDR	logFC	FDR	Spearman r	Spearman P	Spearman r	Spearman P
14:0_872_TAG_C52:4	-0.41	3.72E-01	0.11	8.37E-01	-0.36	2.56E-01	-0.75	4.69E-03
16:0_790_TAG_C46:3	0.19	6.27E-01	0.67	4.70E-02	0.50	9.88E-02	0.67	1.74E-02
16:1_842_TAG_C50:5	0.85	2.49E-02	3.29	2.68E-10	0.73	1.00E-02	0.54	7.25E-02
16:1_870_TAG_C52:5	0.36	4.56E-01	4.65	4.20E-12	0.64	3.01E-02	0.34	2.85E-01
16:1_876_TAG_C52:2	-0.48	3.45E-01	3.31	2.59E-08	-0.41	1.84E-01	-0.68	1.51E-02
18:0_872_TAG_C52:4	0.77	5.55E-02	0.40	3.55E-01	0.71	1.21E-02	0.57	5.43E-02
18:1_822_TAG_C48:1	0.13	8.25E-01	-1.00	3.83E-02	0.66	2.40E-02	0.51	9.18E-02
18:1_846_TAG_C50:3	-0.68	1.81E-01	6.06	1.53E-13	-0.42	1.77E-01	-0.67	1.66E-02
18:1_870_TAG_C52:5	0.71	8.68E-02	0.57	1.81E-01	0.64	2.80E-02	0.60	3.96E-02
18:1_876_TAG_C52:2	-0.56	3.05E-01	0.52	3.54E-01	-0.48	1.15E-01	-0.72	8.54E-03
18:1_906_TAG_C54:1	-0.36	2.89E-01	-0.28	4.48E-01	-0.60	4.28E-02	-0.62	3.03E-02
18:1_TAG_C52_876-339	-0.26	6.51E-01	0.67	2.21E-01	-0.35	2.66E-01	-0.66	1.99E-02
18:2_820_TAG_C48:2	0.43	3.23E-01	0.03	9.56E-01	0.64	3.01E-02	0.48	1.14E-01
18:2_874_TAG_C52:3	-0.43	3.72E-01	1.45	1.63E-03	-0.34	2.87E-01	-0.67	1.82E-02
18:2_898_TAG_C54:5	-0.65	1.13E-01	1.95	1.13E-05	-0.55	7.07E-02	-0.74	6.03E-03
20:0_846_TAG_C50:3	0.26	4.67E-01	0.19	6.39E-01	0.38	2.18E-01	0.62	3.28E-02
20:0_878_TAG_C52:1	0.29	5.10E-01	1.04	1.06E-02	0.61	4.00E-02	0.32	3.07E-01
20:0_908_TAG_C54:0	0.12	8.11E-01	-0.15	7.45E-01	0.60	4.28E-02	0.40	2.03E-01
20:1_876_TAG_C52:2	-0.61	2.55E-01	1.22	1.80E-02	-0.43	1.69E-01	-0.68	1.51E-02
20:2_874_TAG_C52:3	-0.23	6.48E-01	2.22	8.31E-06	-0.37	2.37E-01	-0.68	1.44E-02
20:2_902_TAG_C54:3	-0.49	3.19E-01	1.01	3.01E-02	-0.51	9.36E-02	-0.81	1.32E-03
20:3_872_TAG_C52:4	0.63	1.09E-01	2.21	6.12E-07	0.73	1.00E-02	0.54	7.25E-02
20:4_870_TAG_C52:5	0.63	1.05E-01	1.88	9.38E-06	0.74	8.17E-03	0.51	8.93E-02
20:4_926_TAG_C56:5	-0.67	1.36E-01	0.52	2.66E-01	-0.58	5.21E-02	-0.62	3.15E-02
22:1_932_TAG_C56:2	-0.45	4.00E-01	-0.24	7.02E-01	-0.49	1.10E-01	-0.62	3.15E-02
Cer_16:1	0.19	7.12E-01	1.61	3.63E-04	0.65	2.59E-02	0.39	2.16E-01
Cer_24:0	1.01	3.02E-03	-0.38	2.93E-01	0.62	3.73E-02	0.56	5.62E-02
DAG_36:0_NL_18:0	-0.29	5.64E-01	0.23	6.89E-01	-0.66	2.40E-02	-0.54	7.03E-02
GM3_16:0	-0.29	3.72E-01	-0.36	2.58E-01	-0.62	3.48E-02	-0.44	1.55E-01
PC_32:1	0.48	1.74E-01	0.20	6.36E-01	0.59	4.58E-02	0.58	4.90E-02
PC_38:4	-0.52	2.32E-01	-0.58	1.83E-01	-0.44	1.54E-01	-0.67	1.66E-02
PE_34a:1_718.6	0.43	4.25E-01	0.23	7.03E-01	0.66	2.22E-02	0.56	6.00E-02
PE_40a:0_804.6	-0.39	5.72E-01	-0.69	2.93E-01	-0.38	2.18E-01	-0.59	4.26E-02
PI_34:4	0.60	1.04E-01	1.34	3.32E-04	0.59	4.88E-02	0.49	1.08E-01
PI_40:3	-0.61	2.16E-01	-0.15	7.94E-01	-0.52	8.39E-02	-0.67	1.66E-02
PS_36:0	-0.79	7.82E-02	-0.22	6.89E-01	-0.50	1.04E-01	-0.60	3.96E-02
PS_36:1	-0.26	5.95E-01	-0.02	9.77E-01	-0.28	3.79E-01	-0.58	4.74E-02
PS_38:4	-0.78	1.46E-01	-1.19	2.45E-02	-0.63	3.24E-02	-0.79	2.33E-03
PS_40:3	-1.05	2.40E-02	-0.11	8.41E-01	-0.41	1.93E-01	-0.60	4.11E-02
SPM_18:1	0.18	5.77E-01	0.14	7.03E-01	0.53	7.93E-02	0.61	3.41E-02
SPM_20:1	0.25	4.25E-01	0.15	6.83E-01	0.52	8.87E-02	0.62	3.15E-02
SPM_24:1	-0.31	3.89E-01	-0.20	6.25E-01	-0.27	3.91E-01	-0.58	4.57E-02

Cer, ceramide; SPM, sphingomyelin. Bold font indicates significance ($P < 0.05$).

change in lipid composition within the cells. These findings also suggest that inflammation and insulin resistance in response to PA are associated events. Mechanistically, it has been suggested that saturated fatty acid-induced ceramide biosynthesis occurs in response to TLR4 signaling and mediates insulin resistance (19). However, inhibition of the TLR4-NFκB pathway in our model did not prevent PA-induced impairment of GLUT4 translocation (supplemental Fig. S2), suggesting that although correlated, TLR4-NFκB signaling and insulin resistance are two parallel independent events. Overall, none of the inhibitors of the sphingolipid pathway that we used were able to prevent the detrimental effects of PA, ruling out ceramides and other sphingolipid species as signals linking saturated fatty acids to insulin resistance in L6 muscle cells exposed to PA. This conclusion is not in line with several reports in C2C12 myotubes where myriocin, FB1, and fenretinide did reverse the impaired Akt phosphorylation induced by 0.75 mM of PA; although GLUT4 translocation was not examined in those studies (17, 19). However, in L6 cells exposed to 0.4 mM

PA, conditions very similar to ours, insulin-induced phosphorylation of Akt was not significantly impaired by PA and insulin-induced glucose uptake only partially rescued by myriocin (40). On the other hand, supporting our conclusion, silencing of serine palmitoyltransferase in L6 cells suppressed ceramide synthesis, but did not reverse PA-induced insulin resistance (21). Overexpression of ceramide synthases in L6 myotubes increased ceramides and promoted basal insulin action, but did not affect PA-induced insulin resistance (22). There is also evidence in C2C12 myotubes that increasing oleate concentration deteriorates insulin signaling despite low contents in DAG and ceramides, therefore dissociating ceramide accumulation from insulin resistance (14). It is plausible that the time and concentration of fatty acids as well as the model tested significantly affect the cellular response to PA, but our study and several others report situations where ceramide accumulation is not causally associated with insulin resistance in muscle cells. Thus, there is wide discrepancy in the literature regarding the causal effect of ceramides on reduced insulin

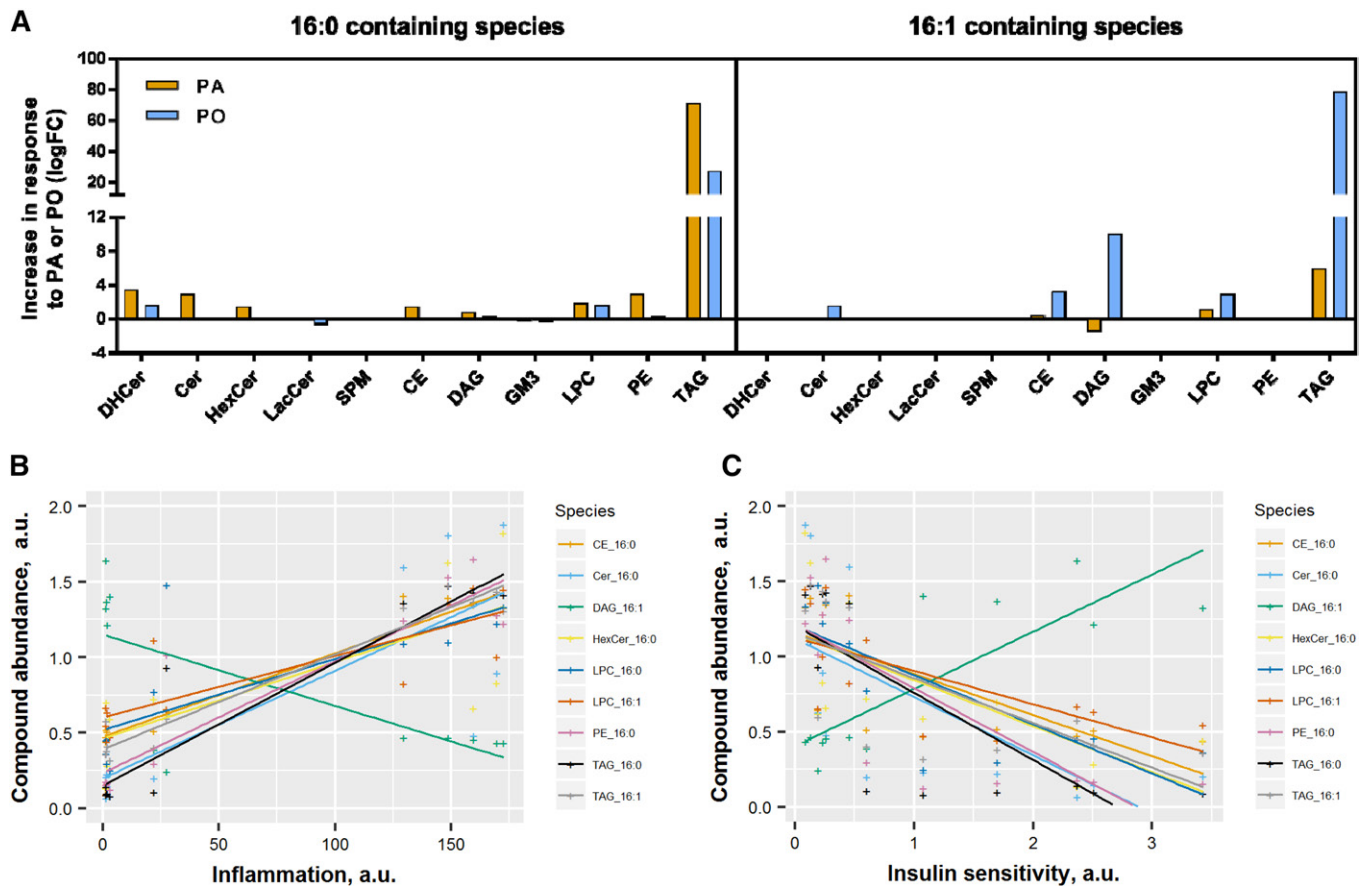


Fig. 8. DAGs containing 16:1 are positively associated with insulin sensitivity. All the 16:0- and 16:1-containing species were analyzed for their response to PA and PO and their correlation with the measurements of insulin sensitivity (surface GLUT4 and Akt activation) and inflammation (*Il6*, *Ccl2* expression, and $\text{I}\kappa\text{B}\alpha$). A: Fold-change induced by PA and PO. B: Correlation with inflammation [$(\text{Il6} + \text{Ccl2})/\text{I}\kappa\text{B}\alpha$ levels]. C: Correlation with insulin sensitivity ($\text{GLUT4} \times \text{Ser}^{473} \times \text{Thr}^{308}$). DHCer, dihydroceramide; HexCer, hexosylceramide; SPM, sphingomyelin; LacCer, lactosylceramide.


signaling evoked by fatty acids. Moreover, when using PA levels that do not cause cellular toxicity, the reduction in insulin-dependent Akt phosphorylation is modest, yet there is substantial impairment in GLUT4 translocation. Altogether, this analysis reveals the need to discern the potential contribution, if any, of endogenous cellular ceramides on the actual outcomes of insulin resistance, rather than focusing only on midway insulin signaling.

Ceramides are not always associated with insulin resistance in vivo

Many reports have shown augmented ceramide and DAG content in the skeletal muscle of obese or diabetic mice and humans, and have therefore suggested that these lipid species play a causal role in the development of insulin resistance (41–44). But a handful of studies did not find any change specifically in skeletal muscle ceramides under high-fat feeding despite their increase in liver, adipose tissue, and plasma (12, 45, 46). In addition, palmitate feeding in cows elevated ceramide levels in plasma and liver, but not in skeletal muscle (13), and intralipid infusion in humans did not significantly change muscle ceramides despite reduced insulin sensitivity (47–49). One of the major differences across these studies is the type of muscle that

was studied: soleus, tibialis, gastrocnemius, or quadriceps in mice and vastus lateralis in human studies. In fact, most studies looking at white muscle did not observe any change in ceramides, while studies comparing white and red muscles consistently saw a bigger change in ceramides in red muscles (50–54). These data suggest that the accumulation of ceramides might be muscle fiber-type specific and therefore would not uniformly support the concept that intramyocellular ceramides are responsible for insulin resistance. In fact, in animal models, muscle ceramide content is not always associated with insulin resistance or even lowered insulin signaling. Ceramide levels rise in muscle during caloric restriction (11, 55), a condition associated with higher skeletal muscle insulin sensitivity. Infusion of oil mixtures composed primarily of unsaturated fatty acids can induce insulin resistance without ceramide production (18, 19, 56). Similarly, both saturated and polyunsaturated fat diets increase muscle ceramide and induce glucose intolerance in mice, but myriocin treatment did not improve glucose tolerance despite a significant reduction in muscle ceramide levels (57). Gene deletion models usually provide a clearer insight than diet interventions, but do not strongly link ceramides to insulin resistance either. Depletion of carnitine palmitoyltransferase (*Cpt1b*) in skeletal

muscle increases ceramide content, but does not impair whole-body insulin response or muscle insulin signaling (58). Ceramide synthase (Cers6)-deficient mice are protected from obesity and glucose intolerance despite no change in C16:0 ceramides and Akt phosphorylation in skeletal muscle (29). Deletion of sphingomyelin synthase 2 in mice improves insulin signaling in liver, adipose tissue, and muscle, but no significant change was observed in muscle sphingolipid content. However, plasma levels of very long-chain fatty acid-containing ceramides were markedly increased in sphingomyelin synthase 2 KO mice and the authors concluded that the elevation of glucose clearance was likely due to indirect mechanisms more than changes in sphingolipid species within tissues (12). Deletion of serine palmitoyltransferase specifically in the adipose tissue is sufficient to prevent liver steatosis and improve whole-body insulin action, despite no change in skeletal muscle ceramide content (59), suggesting that ceramides in muscle are not playing a major role in whole body insulin sensitivity. Another level of complexity arises from recent studies demonstrating important differences in the subcellular localization of ceramides (60). Our study measured total sphingolipid levels and, therefore, cannot exclude that differences in the compartmentalization of ceramides might have significant effects on inflammation and metabolism. Altogether, these findings suggest that improvements in glucose tolerance and insulin sensitivity may not be related to changes in total muscle ceramides. Our in vitro data lend credence to this idea, as the modulation of total intracellular sphingolipid content did not affect insulin sensitivity in L6 myotubes.

In summary, we demonstrate that, in muscle cells in culture, spared of influence by the complex environment of a whole organism, numerous lipid species correlate with indices of insulin resistance and inflammation, such as ceramides, TAG, and S1P. However, normalization of ceramide changes using inhibitors did not rectify insulin sensitivity and inflammation, demonstrating that none of the ceramide species measured play a causative role in the development of insulin resistance, evinced by the key step of insulin-dependent GLUT4 translocation, nor in the development of cell-autonomous inflammation. Surprisingly, our lipidomic analysis also revealed that several TAG species negatively correlate with GLUT4 translocation, Akt phosphorylation, or reduced pro-inflammatory response, while unsaturated 16:1 DAG species positively correlate with insulin responses. Our experimental setup did not test whether these specific TAG and DAG species could play causative roles in regulating muscle insulin sensitivity and inflammation, and specific studies will be needed to explore these potential connections. In conclusion, our findings support the concept that intramyocellular sphingolipid accumulation in response to fatty acids is not a major element in regulating muscle cell-autonomous inflammation and insulin sensitivity. Instead, it is possible that the beneficial effects of ceramide inhibition in vivo are due to changes in sphingolipid metabolites in other tissues, likely the liver and adipose tissue, with consequent secondary potential benefits on skeletal muscle. 

REFERENCES

1. Coen, P. M., and B. H. Goodpaster. 2012. Role of intramyocellular lipids in human health. *Trends Endocrinol. Metab.* **23**: 391–398.
2. Iqbal, J., M. T. Walsh, S. M. Hammad, and M. M. Hussain. 2017. Sphingolipids and lipoproteins in health and metabolic disorders. *Trends Endocrinol. Metab.* **28**: 506–518.
3. Summers, S. A. 2018. Could ceramides become the new cholesterol? *Cell Metab.* **27**: 276–280.
4. Boon, J., A. J. Hoy, R. Stark, R. D. Brown, R. C. Meex, D. C. Henstridge, S. Schenk, P. J. Meikle, J. F. Horowitz, B. A. Kingwell, et al. 2013. Ceramides contained in LDL are elevated in type 2 diabetes and promote inflammation and skeletal muscle insulin resistance. *Diabetes.* **62**: 401–410.
5. Petersen, M. C., and M. J. Jurczak. 2016. CrossTalk opposing view: intramyocellular ceramide accumulation does not modulate insulin resistance. *J. Physiol.* **594**: 3171–3174.
6. Rivas, J. A., D. J. McDonald, N. P. Rice, P. H. Haran, G. G. Dolnikowski, and R. A. Fielding. 2016. Diminished anabolic signaling response to insulin induced by intramuscular lipid accumulation is associated with inflammation in aging but not obesity. *Am. J. Physiol. Regul. Integr. Comp. Physiol.* **310**: R561–R569.
7. Blachnio-Zabielska, A. U., M. Chacinska, M. H. Vendelbo, and P. Zabielski. 2016. The crucial role of C18-Cer in fat-induced skeletal muscle insulin resistance. *Cell. Physiol. Biochem.* **40**: 1207–1220.
8. Park, M., V. Kaddai, J. Ching, K. T. Fridianto, R. J. Sieli, S. Sugiy, and S. A. Summers. 2016. A role for ceramides, but not sphingomyelins, as antagonists of insulin signaling and mitochondrial metabolism in C2C12 myotubes. *J. Biol. Chem.* **291**: 23978–23988.
9. de la Maza, M. P., J. M. Rodriguez, S. Hirsch, L. Leiva, G. Barrera, and D. Bunout. 2015. Skeletal muscle ceramide species in men with abdominal obesity. *J. Nutr. Health Aging.* **19**: 389–396.
10. Tardif, N., J. Salles, C. Guillet, J. Tordjman, S. Reggio, J-F. Landrier, C. Giraudet, V. Patrac, J. Bertrand-Michel, C. Migne, et al. 2014. Muscle ectopic fat deposition contributes to anabolic resistance in obese sarcopenic old rats through eIF2 α activation. *Aging Cell.* **13**: 1001–1011.
11. Skovbro, M., M. Baranowski, C. Skov-Jensen, A. Flint, F. Dela, J. Gorski, and J. W. Helge. 2008. Human skeletal muscle ceramide content is not a major factor in muscle insulin sensitivity. *Diabetologia.* **51**: 1253–1260.
12. Sugimoto, M., Y. Shimizu, S. Zhao, N. Ukon, K. Nishijima, M. Wakabayashi, T. Yoshioka, K. Higashino, Y. Numata, T. Okuda, et al. 2016. Characterization of the role of sphingomyelin synthase 2 in glucose metabolism in whole-body and peripheral tissues in mice. *Biochim. Biophys. Acta.* **1861**: 688–702.
13. Rico, J. E., A. T. Mathews, J. Lovett, N. J. Haughey, and J. W. McFadden. 2016. Palmitic acid feeding increases ceramide supply in association with increased milk yield, circulating nonesterified fatty acids, and adipose tissue responsiveness to a glucose challenge. *J. Dairy Sci.* **99**: 8817–8830.
14. Capel, F., N. Cheraiti, C. Acquaviva, C. Héniq, J. Bertrand-Michel, C. Vianey-Saban, C. Prip-Buus, and B. Morio. 2016. Oleate dose-dependently regulates palmitate metabolism and insulin signaling in C2C12 myotubes. *Biochim. Biophys. Acta.* **1861**: 2000–2010.
15. Chavez, J. A., and S. A. Summers. 2003. Characterizing the effects of saturated fatty acids on insulin signaling and ceramide and diacylglycerol accumulation in 3T3–L1 adipocytes and C2C12 myotubes. *Arch. Biochem. Biophys.* **419**: 101–109.
16. Verma, M. K., A. N. Yateesh, K. Neelima, N. Pawar, K. Sandhya, J. Poornima, M. N. Lakshmi, S. Yogeshwari, P. M. Pallavi, A. M. Oommen, et al. 2014. Inhibition of neutral sphingomyelinases in skeletal muscle attenuates fatty-acid induced defects in metabolism and stress. *Springerplus.* **3**: 255.
17. Bikman, B. T., Y. Guan, G. Shui, M. M. Siddique, W. L. Holland, J. Y. Kim, G. Fabriàs, M. R. Wenk, and S. A. Summers. 2012. Fenretinide prevents lipid-induced insulin resistance by blocking ceramide biosynthesis. *J. Biol. Chem.* **287**: 17426–17437.
18. Holland, W. L., J. T. Brozinick, L-P. Wang, E. D. Hawkins, K. M. Sargent, Y. Liu, K. Narra, K. L. Hoehn, T. A. Knotts, A. Siesky, et al. 2007. Inhibition of ceramide synthesis ameliorates glucocorticoid-, saturated-fat-, and obesity-induced insulin resistance. *Cell Metab.* **5**: 167–179.
19. Holland, W. L., B. T. Bikman, L-P. Wang, G. Yuguang, K. M. Sargent, S. Bulchand, T. A. Knotts, G. Shui, D. J. Clegg, M. R. Wenk, et al. 2011. Lipid-induced insulin resistance mediated by the

- proinflammatory receptor TLR4 requires saturated fatty acid-induced ceramide biosynthesis in mice. *J. Clin. Invest.* **121**: 1858–1870.
20. Lam, Y. Y., G. Hatzinikolas, J. M. Weir, A. Janovská, A. J. McAinch, P. Game, P. J. Meikle, and G. A. Wittert. 2011. Insulin-stimulated glucose uptake and pathways regulating energy metabolism in skeletal muscle cells: the effects of subcutaneous and visceral fat, and long-chain saturated, n-3 and n-6 polyunsaturated fatty acids. *Biochim. Biophys. Acta.* **1811**: 468–475.
 21. Watson, M. L., M. Coghlan, and H. S. Hundal. 2009. Modulating serine palmitoyl transferase (SPT) expression and activity unveils a crucial role in lipid-induced insulin resistance in rat skeletal muscle cells. *Biochem. J.* **417**: 791–801.
 22. Frangioudakis, G., B. Diakanastasis, B-Q. M. Liao, J. T. Saville, N. J. Hoffman, T. W. Mitchell, and C. Schmitz-Peiffer. 2013. Ceramide accumulation in L6 skeletal muscle cells due to increased activity of ceramide synthase isoforms has opposing effects on insulin action to those caused by palmitate treatment. *Diabetologia.* **56**: 2697–2701.
 23. Pillon, N. J., Y. E. Li, L. N. Fink, J. T. Brozinick, A. Nikolayev, M-S. Kuo, P. J. Bilan, and A. Klip. 2014. Nucleotides released from palmitate-challenged muscle cells through pannexin-3 attract monocytes. *Diabetes.* **63**: 3815–3826.
 24. Niu, W., P. J. Bilan, S. Ishikura, J. D. Schertzer, A. Contreras-Ferrat, Z. Fu, J. Liu, S. Boguslavsky, K. P. Foley, Z. Liu, et al. 2010. Contraction-related stimuli regulate GLUT4 traffic in C2C12-GLUT4myc skeletal muscle cells. *Am. J. Physiol. Endocrinol. Metab.* **298**: E1058–E1071.
 25. Ishikura, S., C. N. Antonescu, and A. Klip. 2010. Documenting GLUT4 exocytosis and endocytosis in muscle cell monolayers. *Curr. Protoc. Cell Biol.* **Chapter 15**: Unit 15.15.
 26. Klip, A., Y. Sun, T. T. Chiu, and K. P. Foley. 2014. Signal transduction meets vesicle traffic: the software and hardware of GLUT4 translocation. *Am. J. Physiol. Cell Physiol.* **306**: C879–C886.
 27. Ueyama, A., K. L. Yaworsky, Q. Wang, Y. Ebina, and A. Klip. 1999. GLUT-4myc ectopic expression in L6 myoblasts generates a GLUT-4-specific pool conferring insulin sensitivity. *Am. J. Physiol.* **277**: E572–E578.
 28. Fink, L. N., S. R. Costford, Y. S. Lee, T. E. Jensen, P. J. Bilan, A. Oberbach, M. Blüher, J. M. Olefsky, A. Sams, and A. Klip. 2014. Pro-inflammatory macrophages increase in skeletal muscle of high fat-fed mice and correlate with metabolic risk markers in humans. *Obesity (Silver Spring).* **22**: 747–757.
 29. Turpin, S. M., H. T. Nicholls, D. M. Willmes, A. Mourier, S. Brodessa, C. M. Wunderlich, J. Mauer, E. Xu, P. Hammerschmidt, H. S. Brönneke, et al. 2014. Obesity-induced CerS6-dependent C16:0 ceramide production promotes weight gain and glucose intolerance. *Cell Metab.* **20**: 678–686.
 30. Liang, H., P. Tantiwong, A. Sriwijitkamol, K. Shanmugasundaram, S. Mohan, S. Espinoza, R. A. Defronzo, J. J. Dubé, and N. Musi. 2013. Effect of a sustained reduction in plasma free fatty acid concentration on insulin signalling and inflammation in skeletal muscle from human subjects. *J. Physiol.* **591**: 2897–2909.
 31. Karlsson, H. K., J. R. Zierath, S. Kane, A. Krook, G. E. Lienhard, and H. Wallberg-Henriksson. 2005. Insulin-stimulated phosphorylation of the Akt substrate AS160 is impaired in skeletal muscle of type 2 diabetic subjects. *Diabetes.* **54**: 1692–1697.
 32. Wang, Q., R. Somwar, P. J. Bilan, Z. Liu, J. Jin, J. R. Woodgett, and A. Klip. 1999. Protein kinase B/Akt participates in GLUT4 translocation by insulin in L6 myoblasts. *Mol. Cell. Biol.* **19**: 4008–4018.
 33. Bilan, P. J., V. Samokhvalov, A. Koshkina, J. D. Schertzer, M. C. Samaan, and A. Klip. 2009. Direct and macrophage-mediated actions of fatty acids causing insulin resistance in muscle cells. *Arch. Physiol. Biochem.* **115**: 176–190.
 34. Tan, S-X., Y. Ng, C. C. Meoli, A. Kumar, P-S. Khoo, D. J. Fazakerley, J. R. Junutula, S. Vali, D. E. James, and J. Stöckli. 2012. Amplification and demultiplexing in insulin-regulated Akt protein kinase pathway in adipocytes. *J. Biol. Chem.* **287**: 6128–6138.
 35. Tsuchiya, A., T. Kanno, and T. Nishizaki. 2013. PI3 kinase directly phosphorylates Akt1/2 at Ser473/474 in the insulin signal transduction pathway. *J. Endocrinol.* **220**: 49–59.
 36. Beg, M., N. Abdullah, F. S. Thowfeik, N. K. Altorki, and T. E. McGraw. 2017. Distinct Akt phosphorylation states are required for insulin regulated Glut4 and Glut1-mediated glucose uptake. *eLife.* **6**: e26896.
 37. Tan, S-X., K. H. Fisher-Wellman, D. J. Fazakerley, Y. Ng, H. Pant, J. Li, C. C. Meoli, A. C. F. Coster, J. Stöckli, and D. E. James. 2015. Selective insulin resistance in adipocytes. *J. Biol. Chem.* **290**: 11337–11348.
 38. Othman, A., M. F. Rütli, D. Ernst, C. H. Saely, P. Rein, H. Drexel, C. Porretta-Serapiglia, G. Lauria, R. Bianchi, A. von Eckardstein, et al. 2012. Plasma deoxysphingolipids: a novel class of biomarkers for the metabolic syndrome? *Diabetologia.* **55**: 421–431.
 39. Brozinick, J. T., E. Hawkins, H. Hoang Bui, M-S. Kuo, B. Tan, P. Kievit, and K. Grove. 2013. Plasma sphingolipids are biomarkers of metabolic syndrome in non-human primates maintained on a Western-style diet. *Int. J. Obes. (Lond.).* **37**: 1064–1070.
 40. Miklosz, A., B. Łukaszuk, M. Baranowski, J. Górski, and A. Chabowski. 2013. Effects of inhibition of serine palmitoyltransferase (SPT) and sphingosine kinase 1 (SphK1) on palmitate induced insulin resistance in L6 myotubes. *PLoS One.* **8**: e85547.
 41. Amati, F., J. J. Dubé, E. Alvarez-Carnero, M. M. Edreira, P. Chomentowski, P. M. Coen, G. E. Switzer, P. E. Bickel, M. Stefanovic-Racic, F. G. S. Toledo, et al. 2011. Skeletal muscle triglycerides, diacylglycerols, and ceramides in insulin resistance. *Diabetes.* **60**: 2588–2597.
 42. Bruce, C. R., S. Risis, J. R. Babb, C. Yang, R. S. Lee-Young, D. C. Henstridge, and M. A. Febbraio. 2013. The sphingosine-1-phosphate analog FTY720 reduces muscle ceramide content and improves glucose tolerance in high fat-fed male mice. *Endocrinology.* **154**: 65–76.
 43. Franko, A., J. C. von Kleist-Retzow, M. Böse, C. Sanchez-Lasheras, S. Brodessa, O. Krut, W. S. Kunz, D. Wiedermann, M. Hoehn, O. Stöhr, et al. 2012. Complete failure of insulin-transmitted signaling, but not obesity-induced insulin resistance, impairs respiratory chain function in muscle. *J. Mol. Med. (Berl.).* **90**: 1145–1160.
 44. Moro, C., J. E. Galgani, L. Luu, M. Pasarica, A. Mairal, S. Bajpeyi, G. Schmitz, D. Langin, G. Liebisch, and S. R. Smith. 2009. Influence of gender, obesity, and muscle lipase activity on intramyocellular lipids in sedentary individuals. *J. Clin. Endocrinol. Metab.* **94**: 3440–3447.
 45. Aerts, J. M., R. Ottenhoff, A. S. Powlson, A. Grefhorst, M. van Eijk, P. F. Dubbelhuis, J. Aten, F. Kuipers, M. J. Serlie, T. Wenekes, et al. 2007. Pharmacological inhibition of glucosylceramide synthase enhances insulin sensitivity. *Diabetes.* **56**: 1341–1349.
 46. Matravadia, S., P. Zabielski, A. Chabowski, D. M. Mutch, and G. P. Holloway. 2016. LA and ALA prevent glucose intolerance in obese male rats without reducing reactive lipid content, but cause tissue-specific changes in fatty acid composition. *Am. J. Physiol. Regul. Integr. Comp. Physiol.* **310**: R619–R630.
 47. Chow, L. S., D. G. Mashek, E. Austin, L. E. Eberly, X-M. Persson, M. T. Mashek, E. R. Seaquist, and M. D. Jensen. 2014. Training status diverges muscle diacylglycerol accumulation during free fatty acid elevation. *Am. J. Physiol. Endocrinol. Metab.* **307**: E124–E131.
 48. Hussey, S. E., H. Lum, A. Alvarez, Y. Cipriani, J. Garduño-García, L. Anaya, J. Dube, and N. Musi. 2014. A sustained increase in plasma NEFA upregulates the Toll-like receptor network in human muscle. *Diabetologia.* **57**: 582–591.
 49. Nowotny, B., L. Zahiragic, D. Krog, P. J. Nowotny, C. Herder, M. Carstensen, T. Yoshimura, J. Szendroedi, E. Phielix, P. Schadewaldt, et al. 2013. Mechanisms underlying the onset of oral lipid-induced skeletal muscle insulin resistance in humans. *Diabetes.* **62**: 2240–2248.
 50. Baranowski, M., P. Zabielski, A. U. Błachnio-Zabielska, E. Harasim, A. Chabowski, and J. Górski. 2014. Insulin-sensitizing effect of LXR agonist T0901317 in high-fat fed rats is associated with restored muscle GLUT4 expression and insulin-stimulated AS160 phosphorylation. *Cell. Physiol. Biochem.* **33**: 1047–1057.
 51. Cresser, J., A. Bonen, A. Chabowski, L. E. Stefanyk, R. Gulli, I. Ritchie, and D. J. Dyck. 2010. Oral administration of a PPAR-delta agonist to rodents worsens, not improves, maximal insulin-stimulated glucose transport in skeletal muscle of different fibers. *Am. J. Physiol. Regul. Integr. Comp. Physiol.* **299**: R470–R479.
 52. Holloway, G. P., X. X. Han, S. S. Jain, A. Bonen, and A. Chabowski. 2014. Chronic muscle stimulation improves insulin sensitivity while increasing subcellular lipid droplets and reducing selected diacylglycerol and ceramide species in obese Zucker rats. *Diabetologia.* **57**: 832–840.
 53. Kurek, K., A. Miklosz, B. Łukaszuk, A. Chabowski, J. Górski, and M. Żendzian-Piotrowska. 2015. Inhibition of ceramide de novo synthesis ameliorates diet induced skeletal muscles insulin resistance. *J. Diabetes Res.* **2015**: 154762.
 54. Lee, J. C., I. Y. Kim, Y. Son, S. K. Byeon, D. H. Yoon, J. S. Son, H. S. Song, W. Song, J. K. Seong, and M. H. Moon. 2016. Evaluation of treadmill exercise effect on muscular lipid profiles of diabetic fatty rats by nanoflow liquid chromatography-tandem mass spectrometry. *Sci. Rep.* **6**: 29617.

55. Obanda, D. N., Y. Yu, Z. Q. Wang, and W. T. Cefalu. 2015. Modulation of sphingolipid metabolism with calorie restriction enhances insulin action in skeletal muscle. *J. Nutr. Biochem.* **26**: 687–695.
56. Itani, S. I., N. B. Ruderman, F. Schmieder, and G. Boden. 2002. Lipid-induced insulin resistance in human muscle is associated with changes in diacylglycerol, protein kinase C, and IkappaB-alpha. *Diabetes.* **51**: 2005–2011.
57. Frangioudakis, G., J. Garrard, K. Raddatz, J. L. Nadler, T. W. Mitchell, and C. Schmitz-Peiffer. 2010. Saturated- and n-6 polyunsaturated-fat diets each induce ceramide accumulation in mouse skeletal muscle: reversal and improvement of glucose tolerance by lipid metabolism inhibitors. *Endocrinology.* **151**: 4187–4196.
58. Wicks, S. E., B. Vandanmagsar, K. R. Haynie, S. E. Fuller, J. D. Warfel, J. M. Stephens, M. Wang, X. Han, J. Zhang, R. C. Noland, et al. 2015. Impaired mitochondrial fat oxidation induces adaptive remodeling of muscle metabolism. *Proc. Natl. Acad. Sci. USA.* **112**: E3300–E3309.
59. Chaurasia, B., V. A. Kaddai, G. I. Lancaster, D. C. Henstridge, S. Sriram, D. L. A. Galam, V. Gopalan, K. N. B. Prakash, S. S. Velan, S. Bulchand, et al. 2016. Adipocyte ceramides regulate subcutaneous adipose browning, inflammation, and metabolism. *Cell Metab.* **24**: 820–834.
60. Bionda, C., J. Portoukalian, D. Schmitt, C. Rodriguez-Lafrasse, and D. Ardail. 2004. Subcellular compartmentalization of ceramide metabolism: MAM (mitochondria-associated membrane) and/or mitochondria? *Biochem. J.* **382**: 527–533.